SMAI-JCM
SMAI Journal of Computational Mathematics

Error estimate of the Non-Intrusive Reduced Basis (NIRB) two-grid method with parabolic equations

Elise Grosjean & Yvon Maday

Volume 9 (2023), p. 227-256.
https://doi.org/10.5802/smai-jcm.100

The SMAI Journal of Computational Mathematics is a member of the Centre Mersenne for Open Scientific Publishing
http://www.centre-mersenne.org/
Submissions at https://smai-jcm.centre-mersenne.org/ojs/submission
e-ISSN: 2426-8399

SMAI Journal of Computational Mathematics
Vol. 9, 227-256 (2023)

Error estimate of the Non-Intrusive Reduced Basis (NIRB) two-grid method with parabolic equations

Elise Grosjean [1]
Yvon Maday [2]

[1] Inria Saclay Île-de-France, France
E-mail address: elise.grosjean@inria.fr
[2] Sorbonne Université and Université de Paris Cité, CNRS, Laboratoire Jacques-Louis Lions (LJLL), F-75005 Paris, France and Institut Universitaire de France
E-mail address: yvon.maday@sorbonne-universite.fr.

Abstract. For approximating parametric problem solutions, Reduced Basis Methods (RBMs) are frequently proposed. They intend to reduce the computational costs of High Fidelity (HF) codes while maintaining the HF accuracy. They generally require an offline/online decomposition and a significant modification of the HF code in order for the online computation to be performed in short (or even real) time. We focus on the Non-Intrusive Reduced Basis (NIRB) two-grid method in this paper. Its main feature is the use of the HF code as a "black-box" on a coarse mesh for a new parameter during the online process, followed by an accuracy improvement based on the reduced basis paradigm that is realized in a very short time. Unlike other more intrusive methods, this approach does not necessitate code modification. As a result, it costs significantly less than an HF evaluation. This method was developed for elliptic equations with finite elements and has since then been extended to finite volume schemes.

In this paper, we extend the NIRB two-grid method to parabolic equations. We recover optimal estimates in natural norms, using the heat equation as a model problem and present several numerical results on the heat equation and on the Brusselator problem.

2020 Mathematics Subject Classification. 65K05, 65N08.

Keywords. Non-intrusive reduced basis, parabolic equations, finite elements method.

Supplementary Materials. The paper is accompanied by programs that can be downloaded on the article webnotice (`https://doi.org/10.5802/smai-jcm.100`). Running the codes requires FreeFem++ with IOVTK module and Python3 with package vtk (see Readme therein).

1. Introduction

Reduced Basis Methods (RBMs) can be used to approximate the solutions of a parametric problem for a large number of parameter values (e.g. for applications of parameter fitting), as well as for a single new parameter value (e.g. for real time simulations). They plan to lower the computational costs of High Fidelity (HF) codes while preserving HF accuracy. In order to do so, they rely on a HF traditional code (e.g. finite elements or finite volume methods) and on an offline/online decomposition of the RBM algorithm. They work as driven processes and necessitate well-chosen solutions, called snapshots, that must be computed offline with the HF solver.

Non-Intrusive Reduced Basis (NIRB) methods are an alternative to classical RBMs for approximating the solutions of such problems [9, 10] (see also different NIRB methods [1, 6, 15] from the two-grid method). They may be more practical to implement from an engineering standpoint than other RBMs, as they require the execution of the HF code as a "black-box" solver only, unlike other more intrusive RBMs that require code modification.

Let $\mu \in \mathbb{R}^P$ denotes the parameter of interest of a parametric problem $\mathcal{P}$ in a given set $\mathcal{G}$. The NIRB methods, like most RBMs, rely on the assumption that the solution manifold $\mathcal{S} = \{u(\mu), \mu \in \mathcal{G}\}$ has a

`https://doi.org/10.5802/smai-jcm.100`

small Kolmogorov n-width [27] (in what follows, $u_h(\mu)$ refers to the HF solution for the parameter μ). The snapshots are used offline to construct a linear finite dimensional space, denoted X_h^N, and known as the reduced space, that must be as close as possible to $\mathcal{S}$. The Kolmogorov n-width measures the capacity of approaching the whole solution manifold by linear spaces of dimension n. The online stage then seeks an approximation on this reduced space and must run significantly faster than an HF execution.

We focus in this paper on the NIRB two-grid method [9]. Let us first recall the latter for stationary problems.

1.1. **Reminders on the NIRB two-grid method for stationary problems**

Let Ω be a bounded domain in $\mathbb{R}^d$, with $d \leq 3$ and a smooth enough boundary $\partial\Omega$, and consider a parametric elliptic problem $\mathcal{P}$, well-posed in Ω. For each parameter value $\mu \in \mathcal{G}$, we have a new function $u(\mu) \in V$, where V is a suitable Banach space. In what follows, we consider homogeneous boundary conditions, and $V := H_0^1(\Omega)$, with the associated norm $|\cdot|_{H^1(\Omega)}$.

In the context of a finite element or a finite volume HF solver, the two-grid method involves two partitioned meshes (or "grids"), one fine mesh $\mathcal{M}_h$ and one coarse $\mathcal{M}_H$, where the respective sizes h and H of the meshes are such that $h \ll H$.

The fine mesh is used "offline" to construct basis functions that are employed to build the reduced space with an accuracy that corresponds to the target of the global procedure. These functions form the Reduced Basis (RB) of the reduced space $X_h^N := \text{Span}\{u_h(\mu_i) \,|\, i = 1, \ldots, N\}$, generated using N snapshots. The solution for a new parameter is then roughly and quickly approximated "online", using the coarse mesh. The latter, as well as offline-online decomposition of the algorithm, are crucial components in reducing complexity. Below are recalled the main steps of the NIRB two-grid algorithm:

- **"Offline stage"**:
  The RB functions (or modes) that belong to the reduced space X_h^N are first prepared on the fine mesh $\mathcal{M}_h$ with a Greedy procedure [4, 32] (an alternative is to use a Proper Orthogonal Decomposition (POD) [2, 25]). The Greedy algorithm computes the modes by an iterative selection of some suitable parameters $\mu_1, \ldots, \mu_N \in \mathcal{G}$ and by computing the approximate solutions $u_h(\mu_1), \ldots, u_h(\mu_N)$. Thus, this stage of the algorithm is time-consuming, but it is only performed once, as with other RBMs. It also contains a Gram–Schmidt orthonormalization procedure, which results in N L^2-orthonormalized RB functions, denoted $(\Phi_i^h)_{i=1,\ldots,N}$. In order to improve the accuracy of the online reconstruction (as detailed in Section 4), we solve the following eigenvalue problem:

$$\begin{cases} \text{Find } \Phi^h \in X_h^N, \text{ and } \lambda \in \mathbb{R} \text{ such that:} \\ \forall v \in X_h^N, \displaystyle\int_\Omega \nabla\Phi^h \cdot \nabla v \; d\mathbf{x} = \lambda \int_\Omega \Phi^h \cdot v \; d\mathbf{x}, \end{cases} \tag{1.1}$$

  and we obtain an increasing sequence of eigenvalues λ_i, as well as orthogonal eigenfunctions, still denoted $(\Phi_i^h)_{i=1,\ldots,N}$, orthonormalized in $L^2(\Omega)$ and orthogonal in $H^1(\Omega)$, which define a new basis of the space X_h^N.

  As written above, a coarse approximation for a new parameter $\mu \in \mathcal{G}$ will be used during the online stage. As we will see later, for any parameter $\mu_k,\ k = 1, \ldots, N$, the proposed NIRB approximation differs from the HF $u_h(\mu_k)$, even though this accurate solution is known. Thus, as proposed in [8], we can use a "rectification post-processing" and introduce a rectification matrix, denoted $\mathbf{R}$, defined so as to remove the discrepancies associated to these particular choices of $\mu = \mu_k,\ k = 1, \ldots, N$. As a result, it improves NIRB accuracy for other instances of μ.

In addition to the fine snapshots, the same parameters are used to compute coarse snapshots on $\mathcal{M}_H$. The rows of the matrix $\mathbf{R}$ are then given for $i = 1, \ldots, N$ by

$$\mathbf{R}_i = (\mathbf{A}^T\mathbf{A} + \delta\mathbf{I}_N)^{-1}\mathbf{A}^T\mathbf{B}_i, \tag{1.2}$$

$$\text{where} \quad \forall \mu_k \in \mathcal{G}, \quad A_{k,i} = \int_\Omega u_H(\mu_k) \cdot \Phi_i^h \, d\mathbf{x}, \quad \text{and} \quad B_{k,i} = \int_\Omega u_h(\mu_k) \cdot \Phi_i^h \, \mathbf{x}, \tag{1.3}$$

and where $\mathbf{I}_N$ refers to the identity matrix and δ is a regularization parameter [9].

- **"Online stage"**:
  Then, for a new parameter $\mu \in \mathcal{G}$ for which we want to estimate the solution, a coarse approximation of the latter, denoted $u_H(\mu)$, is computed "online." This coarse approximation is, of course, not of sufficient precision, but it is calculated much faster than the HF one. The NIRB post-processing then improves precision significantly by projecting $u_H(\mu)$ on the RB in a very short run-time [7, 9, 10, 17]. The classical NIRB approximation is given by

$$u_{Hh}^N(\mu) := \sum_{i=1}^N (u_H(\mu), \Phi_i^h) \; \Phi_i^h. \tag{1.4}$$

  where $(\,\cdot\,,\cdot\,)$ denotes the $L^2(\Omega)$-inner product. Now, to further improve the NIRB precision, this approximation can be "rectified" thanks to the rectification matrix $\mathbf{R}$ computed offline. In that case, the NIRB approximation reads

$$R[u_{Hh}^N](\mu) := \sum_{i,j=1}^N R_{ij} \; (u_H(\mu), \Phi_j^h) \; \Phi_i^h. \tag{1.5}$$

  Note that, when the relaxation parameter δ is equal to 0 the rectification process allows to retrieve the fine coefficients from the coarse ones (1.3) for the parameters $\mu = \mu_k$, $k = 1, \ldots, N$. In other words, with $\delta = 0$, we have

$$R[u_{Hh}^N](\mu_k) = u_h(\mu_k), \quad k = 1, \ldots, N.$$

The two-grid method has been developed and analyzed for elliptic equations in the context of FEM (with Céa's and Aubin–Nitsche's lemmas) in [8]. In this context, the following energy-error estimate has been proven

$$|u(\mu) - u_{Hh}^N(\mu)|_{H^1(\Omega)} \leq \varepsilon(N) + C_1 h + C_2(N) H^2, \tag{1.6}$$

where C_1 and C_2 are constants independent of h and H, and C_2 depends on N only. The term $\varepsilon(N)$ depends on a proper choice of the RB space as a surrogate for the best approximation space associated to the Kolmogorov N-width. It decreases when N increases and it measures the error between the fine solution and its projection on X_h^N, given by

$$\left| u_h(\mu) - \sum_{i=1}^N (u_h(\mu), \Phi_i^h) \; \Phi_i^h \right|_{H^1(\Omega)}. \tag{1.7}$$

The second and third terms in (1.6), $C_1 \; h$ and $C_2(N) \; H^2$, respectively, are contributions obtained by applying Céa's lemma on the HF solutions and Aubin–Nitsche's lemma on the coarse grid approximation of $u(\mu)$. Note that since the constant C_2 increases with N, a trade-off must be made between increasing N and keeping a constant C_2 as low as possible to obtain an accurate approximation.

The estimate (1.6) proves that, in the elliptic context with FEM, if the coarse mesh size is chosen so that $H^2 = h$ and if $\varepsilon(N)$ is small enough, the optimal H^1 convergence rate is recovered. Furthermore, it has been numerically shown that for a large range of H values, the rectification post-treatment allows for the recovery of the fine solution accuracy while greatly reducing the run-time cost.

This two-grid method has also been generalized and analyzed in the context of finite volume schemes [17], in which a surrogate to Aubin–Nitsche's is used.

1.2. **Motivation and earlier works**

The treatment of time-dependent equations by RB techniques is not obvious, particularly because a classical projection-based RBM does not guarantee a stable approximation, and because the solution manifold, obtained as time and parameters vary, must be of low dimension, which is not always the case for several phenomena (for example convection-dominated problems [5]). For a general overview of RBMs in the context of time-dependent problems, see [24]. Although NIRB strategies for time-dependent equations are still in the early stages of development, we would like to mention the following NIRB techniques, different from the two-grid algorithm, that have been applied to time-dependent problems:

- Neural network framework has been used to learn the reduced operators, as in the POD-DL-ROM algorithm [14] or in [12];
- Interpolations with Radial Basis Functions (POD-RBF) have also been operated in [35].
- The time-parameter grid structure has been exploited, as in [11], where RBF with two level POD extraction is employed, or in [19], where a map is constructed between the time-parameter grid values and the RB projection coefficients through a regression model.
- Also, in the context of inverse problems, the Parameterized-Background-Data-Weak (PBDW) has been generalized to parabolic equations in [22].

It should be noted that in [18], the NIRB two-grid method has recently been adapted to solve the sensitivity analysis equations with a regression model. As it was presented in the previous subsection, the two-grid method is of simple implementation and can be used for a variety of PDEs and approximations; furthermore, because it is non-intrusive, it is suitable for a wide range of problems. To the best of our knowledge, this method has not yet been studied or implemented in the context of time-dependent problems [7, 9, 10, 33], aside from the sensitivity analysis framework [18].

This paper is about the application of NIRB to time-dependent problems and its numerical analysis in the context of parabolic equations. The rest of this paper is organized as follows: The mathematical context is described in Section 2. We define the NIRB approximation, with and without the adapted rectification post-treatment, in the context of parabolic equations, as an extension of (1.4) and (1.5) in Section 3. We prove then theoretically, in the Section 4, that we recover optimal error estimates in $L^\infty(0,T;H^1(\Omega))$ on a model problem, that of the heat equation. Theorem 4.1 is our main convergence result. Finally, the implementation is discussed in the last Section 5, and the theoretical results are illustrated with numerical results on the NIRB method with and without the rectification post-treatment.

In the next sections, C will denote various positive constants independent of the size of the meshes h and H and of the parameter μ, and $C(\mu)$ will denote constants independent of the sizes of the meshes h and H but dependent of μ.

2. **Mathematical Background**

2.1. **The continuous problem**

We first consider the following heat equation on the domain Ω with homogeneous Dirichlet conditions, which takes the form

$$\begin{cases} u_t - \mu\Delta u = f, & \text{in } \Omega\times\,]0,T], \\ u(\,\cdot\,,0) = u^0, & \text{in } \Omega, \\ u(\,\cdot\,,t) = 0, & \text{on } \partial\Omega\times\,]0,T], \end{cases} \tag{2.1}$$

where $f \in L^2(\Omega \times [0,T])$, while $u^0 \in H_0^1(\Omega)$ and $0 < \mu \in \mathcal{G} \subset \mathbb{R}^+$ is the parameter. For almost any $t > 0$, the solution $u(\,\cdot\,,t) \in H_0^1(\Omega)$, and $u_t(\,\cdot\,,t) \in L^2(\Omega)$ stands for the derivative of u with respect to time. In Section 4, we denote by $u(\mathbf{x},t;\mu)$ (or $u(\mu)$) the solution of (2.1) with the parameter μ. Note that the initial condition may also depend on μ.

We use the conventional notations for space-time Sobolev spaces [28]

$$L^p(0,T;V0) := \left\{ u(\mathbf{x},t) \;\middle|\; \|u\|_{L^p(0,T;V)} := \left(\int_0^T \|u(\,\cdot\,,t)\|_V^p \; dt \right)^{1/p} < \infty \right\},\ 1 \le p < \infty,$$

$$L^\infty(0,T;V) := \left\{ u(\mathbf{x},t) \;\middle|\; \|u\|_{L^\infty(0,T;V)} := \operatorname{ess}\sup_{0\le t\le T} \|u(\,\cdot\,,t)\|_V < \infty \right\},$$

where V is a real Banach space with an associated norm $\|\cdot\|_V$. As in the previous Section 1.1, we consider $V := H_0^1(\Omega)$, with the associated norm $|\cdot|_{H^1(\Omega)}$. The variational form of (2.1) is given by:

$$\begin{cases} \text{Find } u \in L^2(0,T;H_0^1(\Omega)) \text{ with } u_t \in L^2(0,T;H^{-1}(\Omega)) \text{ such that} \\ (u_t(t,\,\cdot\,),v) + a(u(t,\,\cdot\,),v;\mu) = (f(t,\,\cdot\,),v),\ \forall v \in H_0^1(\Omega) \text{ and a.e. } t \in (0,T), \\ u(\,\cdot\,,0) = u^0,\ \text{in } \Omega, \end{cases} \tag{2.2}$$

where a is given by

$$a(w,v;\mu) = \int_\Omega \mu \nabla w(\mathbf{x}) \cdot \nabla v(\mathbf{x}) \; d\mathbf{x}, \quad \forall w,v \in H_0^1(\Omega). \tag{2.3}$$

We remind that (2.2) is well posed (see [13] for the existence and the uniqueness of solutions to problem (2.2)) and we refer to the notations of [13].

2.2. **The various discretizations**

As in previous work on the NIRB FEM applied to elliptic equations [8], described in Section 1.1, we consider one fine mesh $\mathcal{M}_h$ for computing "offline" snapshots associated with few parameter values and one coarse mesh $\mathcal{M}_H$ for the coarse solution, with sizes denoted h and H, respectively (with $h \ll H$). The size h (respectively H) is defined as

$$h = \max_{K\in\mathcal{M}_h} h_K \text{ (respectively } H = \max_{K\in\mathcal{M}_H} H_K), \tag{2.4}$$

where the diameter h_K (or H_K) of any element K in a mesh is equal to $\sup x,y \in K|x-y|, K \in M_h$ (or $\in M_H$).

These grids are used for the spatial discretizations of the weak formulation of problem (2.1). We employ e.g. $\mathbb{P}_1$ finite elements to discretize in space, so let V_h and V_H be continuous piece-wise linear finite element functions (on fine and coarse mesh, respectively) that vanish on the boundary $\partial\Omega$. We consider the projection operator P_h^1 on V_h (P_H^1 on V_H is defined similarly) which is given by

$$(\nabla P_h^1 u, \nabla v) = (\nabla u, \nabla v), \quad \forall v \in V_h. \tag{2.5}$$

In the context of time-dependent problems, a time stepping method of finite difference type is used to get a fully discrete approximation of the solution. We consider two different time grids for the NIRB construction :

- One time grid, denoted F, is employed for the HF snapshots construction. To avoid making notations more cumbersome, we will consider a uniform time step Δt_F. The time levels can be written $t^n = n\ \Delta t_F$, where $n \in \mathbb{N}^*$.
- Another time grid, denoted G, is used for the coarse solution. By analogy with the fine grid, we consider a uniform grid with time step Δt_G. Now, the time levels are written $\widetilde{t}^m = m\ \Delta t_G$, where $m \in \mathbb{N}^*$.

As in the previous analysis with elliptic equations, the NIRB algorithm is designed to recover the optimal estimate in space from a coarse grid approximation. However, there is no such argument as the Aubin–Nitsche lemma for time stepping methods improving the time convergence rate, so we must consider time discretizations that provide the same precision with larger time steps. Thus, we consider a higher order time scheme for the coarse solution. We will use an Euler scheme (first order approximation) for the HF solutions and a Crank–Nicolson scheme (second order approximation) for the coarse solutions with our model problem. As a result, we must employ two types of notations for the discretized solutions:

- $u_h(\mathbf{x},t)$ and $u_H(\mathbf{x},t)$ that respectively denote the fine and coarse solutions of the spatially semi-discrete solution, at time $t \geq 0$.
- $u_h^n(\mathbf{x})$ and $u_H^m(\mathbf{x})$ that respectively denote the fine and coarse full-discretized solutions at time $t^n = n \times \Delta t_F$ and $\widetilde{t}^m = m \times \Delta t_G$.

Remark 2.1. To simplify the notations, we consider that both time grids end at time T here,

$$T \;=\; N_T\ \Delta t_F \;=\; M_T\ \Delta t_G.$$

The semi-discrete form of the variational problem (2.2) writes for the fine mesh (similarly for the coarse mesh):

$$\begin{cases} \text{Find } u_h(t) = u_h(\,\cdot\,,t) \in V_h \text{ for } t \in [0,T] \text{ such that} \\ (\partial_t u_h(t), v_h) + a(u_h(t), v_h; \mu) = (f(t), v_h),\ \forall v_h \in V_h \text{ and } t \in\,]0,T], \\ u_h(\,\cdot\,,0) \;=\; u_h^0 \;=\; P_h^1(u^0). \end{cases} \tag{2.6}$$

The full discrete form of the variational problem (2.2) for the fine mesh with implicit Euler scheme writes:

$$\begin{cases} \text{Find } u_h^n \in V_h \text{ for } n = 0,\dots,N_T \text{ such that} \\ (\overline{\partial} u_h^n, v_h) + a(u_h^n, v_h; \mu) = (f(t^n), v_h),\ \forall v_h \in V_h \text{ and } n = 1,\dots,N_T, \\ u_h(\,\cdot\,,0) \;=\; u_h^0, \end{cases} \tag{2.7}$$

where the time derivative in the variational form of the problem (2.6) has been replaced by a backward difference quotient, $\overline{\partial} u_h^n = \frac{u_h^n - u_h^{n-1}}{\Delta t_F}$. Note that for the initial condition u_h^0, another optimal choice may be the orthogonal projection of u_0 onto V_h (respectively V_H) with respect to the inner product in $L^2(\Omega)$.

For the coarse mesh with Crank–Nicolson scheme, and with the notation $\overline{\partial} u_H^m = \frac{u_H^m - u_H^{m-1}}{\Delta t_G}$, it becomes:

$$\begin{cases} \text{Find } u_H^m \in V_H \text{ for } m = 0,\dots,M_T, \text{ such that} \\ (\overline{\partial} u_H^m, v_H) + a(\frac{u_H^m + u_H^{m-1}}{2}, v_H; \mu) = (f(\widetilde{t}^{m-\frac{1}{2}}), v_H),\ \forall v_H \in V_H \text{ and } m = 1,\dots M_T, \\ u_H(\,\cdot\,,0) \;=\; u_H^0, \end{cases} \tag{2.8}$$

where $\widetilde{t}^{m-\frac{1}{2}} = \frac{\widetilde{t}^m + \widetilde{t}^{m-1}}{2}$.

Let us recall a few results from [34], on the FEM classical estimates and on both finite difference schemes used. These results will be useful for the proof of Theorem 4.1. In [34], these estimates are proven on the solution of the heat equation without considering the dependence on $\mu \in \mathcal{G}$ for the diffusion coefficient. These precised estimates can be obtained by following the same steps as in [34]. In Appendix B, we detail the proof on the H_0^1 estimate of Theorem 2.5 in order to highlight the μ-dependence of the bound.

If $u^0 \in H^2(\Omega)$ and $\|u_h^0 - u^0\|_{L^2(\Omega)} \leq Ch^2 \|u^0\|_{H^2(\Omega)}$, the following estimates are well known to hold:

Theorem 2.2 (Corollary of [34, Thm. 1.2]). *Let Ω be a convex polyhedron. Let $u \in W^{1,1}(0,T;H^2(\Omega))$ be the solution of (2.1) and u_h be the semidiscretized variational form (2.6). Then*

$$\forall t \geq 0, \quad \|u(t) - u_h(t)\|_{L^2(\Omega)} \leq Ch^2 \left[\left\| u^0 \right\|_{H^2(\Omega)} + \int_0^t \|u_t\|_{H^2(\Omega)} \, ds \right], \tag{2.9}$$

where C does not depend on μ.

Once fully discretized on a fine mesh with the backward Euler Galerkin method, the estimate (2.9) is replaced by the estimate below.

Theorem 2.3 (Corollary of [34, Thm. 1.5]). *Let Ω be a convex polyhedron, and let the solution of (2.1) u be in $W^{1,1}(0,T;H^2(\Omega)) \cap W^{2,1}(0,T;L^2(\Omega))$ and u_h^n be the solution of (2.7). We have*

$$\forall n = 0, \ldots, N_T,$$
$$\|u(t^n) - u_h^n\|_{L^2(\Omega)} \leq Ch^2 \left[\left\| u^0 \right\|_{H^2(\Omega)} + \int_0^{t^n} \|u_t\|_{H^2(\Omega)} \, ds \right] + C \, \Delta t_F \int_0^{t^n} \|u_{tt}\|_{L^2(\Omega)} \, ds. \tag{2.10}$$

On the energy error estimate, the following theorems hold.

Theorem 2.4 (Corollary of [34, Thm. 1.4]). *Let Ω be a convex polyhedron, and let the solution of (2.1) u be in $H^1(0,T;H^1(\Omega)) \cap L^2(0,T;H^2(\Omega))$ and u_h be the semidiscretized variational form (2.6). We have*

$$\forall t \geq 0, \quad \|\nabla u(t) - \nabla u_h(t)\|_{L^2(\Omega)} \leq C(\mu) h \left[\left\| u^0 \right\|_{H^2(\Omega)} + \|u(t)\|_{H^2(\Omega)} + \left(\int_0^t \|u_t\|_{H^1(\Omega)}^2 \, ds \right)^{1/2} \right]. \tag{2.11}$$

The estimate (2.11) with the full discretization leads to the following theorem.

Theorem 2.5. *Let Ω be a convex polyhedron. Let $u \in H^2(0,T;H^1(\Omega)) \cap H^1(0,T;H^2(\Omega))$ be the solution of (2.1) and let u_h^n be the fully-discretized solution of the variational form (2.6). We have*

$$\forall n = 0, \ldots N_T, \quad \|\nabla u_h^n - \nabla u(t^n)\|_{L^2(\Omega)} \leq C(\mu) h \left[\left\| u^0 \right\|_{H^2(\Omega)} + \left(\int_0^{t^n} \|u_t\|_{H^2(\Omega)}^2 \, ds \right)^{1/2} \right]$$
$$+ C(\mu) \, \Delta t_F \left(\int_0^{t^n} \|\nabla u_{tt}\|_{L^2(\Omega)}^2 \, ds \right)^{1/2}. \tag{2.12}$$

Finally, using the Crank–Nicolson scheme, we can recover the estimate in H^2 and Δt_G^2 in the L^2 norm

Theorem 2.6 (Corollary of [34, Thm. 1.6]). *Let Ω be a convex polyhedron, and let the solution of (2.1) u be in $H^2(0,T;H^2(\Omega)) \cap H^3(0,T;L^2(\Omega))$. Let u_H^m be the solution given by (2.8), associated to Crank–Nicolson discretization on the time and spatial coarse grids. Let $\|u_H^0 - u^0\|_{L^2(\Omega)} \leq CH^2 \|u^0\|_{H^2(\Omega)}$, then*

$$\forall m = 0, \ldots, M_T,$$
$$\left\| u(\widetilde{t}^m) - u_H^m \right\|_{L^2(\Omega)} \leq C \; H^2 \left[\left\| u^0 \right\|_{H^2(\Omega)} + \int_0^{\widetilde{t}^m} \|u_t\|_{H^2(\Omega)} \, ds \right]$$
$$+ C \; \Delta t_G^2 \left[\left(\int_0^{\widetilde{t}^m} \|u_{ttt} \, ds\|_{L^2(\Omega)}^2 \right)^{1/2} + \left(\int_0^{\widetilde{t}^m} \|\Delta u_{tt}\|_{L^2(\Omega)}^2 \, ds \right)^{1/2} \right]. \tag{2.13}$$

Now, let $\widetilde{u_H}^n$ be the quadratic interpolation in time of the coarse solution at time $t^n \in I_m = [\widetilde{t}^{m-1}, \widetilde{t}^m]$ defined on $[\widetilde{t}^{m-2}, \widetilde{t}^m]$ from the values u_H^{m-2}, u_H^{m-1}, and u_H^m, for all $m = 2, \ldots, M_T$. To this end, we define the parabola on $[\widetilde{t}^{m-2}, \widetilde{t}^m]$ with the values $u_H^{m-2}, u_H^{m-1}, u_H^m$:

For $m \geq 2$, $\forall n \in I_m = [\widetilde{t}^{m-1}, \widetilde{t}^{m}]$,

$$\begin{aligned}\widetilde{u_H}^n(\mu) = &\frac{u_H^{m-2}(\mu)}{(\widetilde{t}^m - \widetilde{t}^{m-2})(\widetilde{t}^{m-2} - \widetilde{t}^{m-1})}\big[-(t^n)^2 + (\widetilde{t}^{m-1} + \widetilde{t}^m)t^n - t^{m-1}t^m\big] \\ &+ \frac{u_H^{m-1}(\mu)}{(\widetilde{t}^{m-2} - \widetilde{t}^{m-1})(\widetilde{t}^{m-1} - \widetilde{t}^m)}\big[-(t^n)^2 + (\widetilde{t}^{m} + \widetilde{t}^{m-2})t^n - t^{m}t^{m-2}\big] \\ &+ \frac{u_H^{m}(\mu)}{(\widetilde{t}^{m-1} - \widetilde{t}^m)(\widetilde{t}^m - \widetilde{t}^{m-2})}\big[-(t^n)^2 + (\widetilde{t}^{m-2} + \widetilde{t}^{m-1})t^n - t^{m-2}t^{m-1}\big]. \end{aligned} \tag{2.14}$$

For $t^n \in I_1 = [\widetilde{t}^0, \widetilde{t}^1]$, we use the same parabola defined by the values u_H^0, u_H^1, u_H^2 as the one used over $[\widetilde{t}^1, \widetilde{t}^2]$. Note that we choose this interpolation in order to keep an approximation of order 2 for all time steps in F (it works also with other quadratic interpolations). With this interpolated approximation, we have the following result.

Corollary 2.7 (of Theorem 2.6)**.** *Under the assumptions of Theorem 2.6, let $\widetilde{u_H}^n$ be the quadratic interpolation in time of the coarse solution, defined above, then*

$\forall n = 0, \ldots, N_T$,

$$\begin{aligned}\left\|u(\widetilde{t}^n) - \widetilde{u_H}^n\right\|_{L^2(\Omega)} \leq C(\mu)H^2\left[\left\|u^0\right\|_{H^2(\Omega)} + \int_0^{\widetilde{t}^m} \|u_t\|_{H^2(\Omega)}\ ds\right] \\ + C(\mu)\Delta t_G^2\left[\left(\int_0^{\widetilde{t}^m} \|u_{ttt}\ ds\|_{L^2(\Omega)}^2\right)^{1/2} + \left(\int_0^{\widetilde{t}^m} \|\Delta u_{tt}\|_{L^2(\Omega)}^2\ ds\right)^{1/2}\right]. \end{aligned} \tag{2.15}$$

We will also need the following inverse inequality [34]

Theorem 2.8 (Inverse inequality)**.** $\forall v_h \in V_h$,

$$\|\nabla v_h\|_{L^2(\Omega)} \leq Ch^{-1}\|v_h\|_{L^2(\Omega)}. \tag{2.16}$$

Let us proceed with the NIRB algorithm description in the context of parabolic equations.

3. The Non-Intrusive Reduced Basis method (NIRB) in the context of parabolic equations

This section describes the main steps of the two-grid method algorithm in the context of parabolic equations, and especially, how to define the RB using a Greedy algorithm [4] (greedy both in parameter selection and in time) or a POD-Greedy [20, 21, 26]. For evolution PDEs, a single solution associated with a parameter $\mu \in \mathcal{G}$ is made up of a sequence of potentially hundreds of snapshots over time (each snapshot being an HF finite element approximation in space at a time $t^n,\ n = 0, \ldots, N_T$). As a result, each step in the Greedy algorithm is combined with a temporal compression step, performed by a POD in the latter version. Let us go over the different steps of our offline-online decomposition. The first four points are completed offline, while the remaining three points are executed online.

- **"Offline step"**

  (1) We define $\mathcal{G}_{\text{train}} = \bigcup_{i\in\{1,\ldots,N_{\text{train}}\}} \mu_i$ and assume that it is large enough so that the space spanned by the snapshots $\{u(\cdot,\cdot;\mu_i)\}_{i\in\{1,\ldots N_{\text{train}}\}}$ is "representative" enough of the whole manifold

  $$\mathcal{S} = \{u^n(\mu,t), \mu \in \mathcal{G},\ n = 0, \ldots, N_T\}.$$

  We refer to [29] for a Greedy algorithm with adaptive choice of optimal training set, adapted to a target accuracy.

(2) From the training parameters $(\mu_i)_{i\in\{1,\dots,N_{\text{train}}\}}$, we compute HF snapshots $\{u_h^n(\mu_i)\}_{i\in\{1,\dots N_{\text{train}}\}}$ with the HF solver.

(3) We generate the RB functions (time-independent) $(\Phi_i^h)_{i=1,\dots,N}$ through a POD-Greedy algorithm from the above snapshots, as presented in Algorithm 3, in Appendix A, or a full Greedy algorithm as in Algorithm 1, that contains a Gram–Schmidt orthonormalization procedure. In that case, for each selected parameter μ_i, $i = 1,\dots,N_\mu$, a small number N^i of snapshots with different time steps are chosen (see Algorithm 1 with the setting $N_\mu = N$ to simplify notations). The RB space, with $N := \sum_{i=1}^{N_\mu} N^i$, is defined as

$$X_h^N := \text{Span}\left\{ u_h^{n_i^j}(\mu_i) \,\middle|\, n_i^j \subset \{0,\dots,N_T\},\ i = 1,\dots,N_\mu,\ j = 1,\dots,N^i \right\}. \tag{3.1}$$

In the following Greedy algorithm, a tolerance threshold is used instead of an a priori given number of modes.

Algorithm 1 Greedy algorithm

Input tol, $\{u_h^n(\mu_i)\}$ with $\mu_i \in \mathcal{G}_{\text{train}},\ n \in F = \{0,\dots,N_T\}\}$.
Output: Reduced basis $\{\Phi_1^h,\dots,\Phi_N^h\}$.

Choose $\mu_1, n_1 = \text{argmax}_{\mu\in\mathcal{G}_{\text{train}},\ n\in F} \left\|u_h^n(\mu)\right\|_{L^2(\Omega)}$.
Set $\Phi_1^h = \frac{u_h^{n_1}(\mu_1)}{\left\|u_h^{n_1}(\mu_1)\right\|_{L^2}}$.
Set $\mathcal{G}_1 = \{\mu_1, n_1\}$ and $X_h^1 = \text{span}\{\Phi_1^h\}$.
for $k = 2$ to N **do**:
$\mu_k, n_k = \text{argmax}_{\mu\in\mathcal{G}_{\text{train}}\setminus\mathcal{G}_{k-1}, n\in F} \left\|u_h^n(\mu) - P^{k-1}(u_h^n(\mu))\right\|_{L^2}$,
with $P^{k-1}(u_h(\mu)) := \sum_{i=1}^{N_{k-1}} (u_h(\mu), \Phi_i^h)_{L^2}\Phi_i^h$.
Compute $\widetilde{\Phi_k^h} = u_h^{n_k}(\mu_k) - \sum_{i=1}^{k-1}(u_h^n(\mu_k), \Phi_i^h)_{L^2(\Omega)}\Phi_i^h$ and set $\Phi_k^h = \frac{\widetilde{\Phi_k^h}}{\left\|\widetilde{\Phi_k^h}\right\|_{L^2(\Omega)}}$.
Set $\mathcal{G}_k = \mathcal{G}_{k-1} \cup \{\mu_k\}$ and $X_h^k = X_h^{k-1} \oplus \text{span}\{\Phi_k^h\}$.
Stop when $\left\|u_h^n(\mu) - P^{k-1}(u_h^n(\mu))\right\|_{L^2} \le tol,\ \forall\mu \in \mathcal{G}_{\text{train}},\ \forall n \in F$.
end for

Note that the Greedy algorithm is generally less expensive (thanks to a posteriori error estimates), but for time dependent problems, the POD-Greedy might be more reasonable when the snapshots are computed for all time steps since it avoids performing an additional forloop on the time steps [21]. Yet, in this algorithm, since an additional rectification post-treatment can be performed (detailed later), the use of a Greedy algorithm (with an additional selection over the time steps) Algorithm 1 makes more sens and might lead to more accurate approximations [16].
After generating the RB functions, we solve the following eigenvalue problem:

$$\begin{cases} \text{Find } \Phi^h \in X_h^N, \text{ and } \lambda \in \mathbb{R} \text{ such that:} \\ \forall v \in X_h^N, \int_\Omega \nabla\Phi^h \cdot \nabla v \, d\mathbf{x} = \lambda \int_\Omega \Phi^h \cdot v \, d\mathbf{x}, \end{cases} \tag{3.2}$$

where $X_h^N = \text{Span}\{\Phi_1^h,\dots,\Phi_N^h\}$. We get an increasing sequence of eigenvalues λ_i, and orthogonal eigenfunctions, still denoted $(\Phi_i^h)_{i=1,\dots,N}$, which do not depend on time, orthonormalized in $L^2(\Omega)$ and orthogonalized in $H^1(\Omega)$. Note that with the Gram–Schmidt process, we only obtain an L^2-orthonormalized RB.

(4) To perform the rectification post-treatment, we generate the equivalent coarse snapshots and rectification matrices with algorithm 2, in analogy with the elliptic case. The coarse snapshots, which have the same parameters as for the HF one, are now quadratically interpolated in time (2.14). We resort to the following algorithm.

Algorithm 2 Offline rectification post-treatment

Input: $\{(u_h^n(\mu_i),\ \text{with}\ \mu_i \in \mathcal{G}_{\text{train}}, n \in F\}$; $\{u_H^m(\mu_i),\ \text{with}\ \mu_i\ \in\ \mathcal{G}_{\text{train}} \subset\ \mathcal{G}, m \in G\}$;
RB $\{\Phi_i^h\}_{i=1,\dots,N}$.
Output: Rectification matrices $R_{i,j}^n, 1 \le i,j \le N,\ n = 0,\dots,N_T$.

Realize the quadratic interpolation of the coarse snapshots in time, denoted $\widetilde{u_H}^n,\ \ n \in F$ with (2.14).
for $n = 0,\dots,N_T$ **do**
Calculate the fine and coarse coefficients
$\forall i = 1,\dots,N,$ and $\forall \mu_k \in \mathcal{G}_{\text{train}},\ A_{k,i}^n = \int_\Omega \widetilde{u_H}^n(\mu_k) \cdot \Phi_i^h\ d\mathbf{x}$, and $B_{k,i}^n = \int_\Omega u_h^n(\mu_k) \cdot \Phi_i^h\ d\mathbf{x}$,
For $i = 1,\dots,N$, set $\mathbf{R}_i^n = ((\mathbf{A}^n)^T\mathbf{A}^n + \delta \mathbf{I}_N)^{-1}(\mathbf{A}^n)^T\mathbf{B}_i^n$.
end for

Remark 3.1. In algorithm 1, the term

$$\left\| u_h^n(\mu) - P^{k-1}(u_h^n(\mu)) \right\|_{L^2(\Omega)} \tag{3.3}$$

can be calculated either with a set of training snapshots as presented in Algorithm 1 or evaluated with an a posteriori estimate. Since at each step k, all sets added in the basis are in the orthogonal complement of X_h^{k-1}, it yields an L^2 orthogonal basis without further processing. In practice, the algorithm is halted with a stopping criterion such as an error threshold or a maximum number of basis functions to generate.

Remark 3.2. Every time step has its own rectification matrix. Indeed, in our experiments, the results obtained with a global rectification matrix were less accurate. Because there are several time steps for each parameter in $\mathcal{G}_{\text{train}}$, we have $N_{\text{train}} \le N$ in our context. Hence, $\forall n \in \{1,\dots,N_T\},\ \mathbf{A}^n \in \mathbb{R}^{N_{\text{train}} \times N}$ is a rectangular "flat" matrix, and $(\mathbf{A}^n)^T\mathbf{A}^n$ is not invertible and requires the parameter δ for the inversion. Note that in previous NIRB two-grid studies, the parameter δ was used only as a regularization parameter.

- **"Online step"**

(5) Now for the online part, we solve the coarse problem (e.g. (2.1) for the heat equation) on $\mathcal{M}_H$ for a new parameter $\mu \in \mathcal{G}$, at each time step $m = 0,\dots,M_T$.
(6) We quadratically interpolate in time the coarse solution on the fine time grid with (2.14).
(7) Then, we linearly interpolate $\widetilde{u_H}^n(\mu)$ on $\mathcal{M}_h$ in order to compute the $L^2(\Omega)$-inner product with the RB functions. The approximation used in the two-grid method is

$$\text{For } n = 0,\dots,N_T, \quad u_{Hh}^{N,n}(\mu) := \sum_{i=1}^{N} (\widetilde{u_H}^n(\mu), \Phi_i^h)\ \Phi_i^h, \tag{3.4}$$

and with the rectification post-treatment step [9, 17], it becomes

$$R^n[u_{Hh}^N](\mu) := \sum_{i=1}^{N} R_{ij}^n\ (\widetilde{u_H}^n(\mu), \Phi_j^h)\ \Phi_i^h, \tag{3.5}$$

where R^n is the rectification matrix at time t^n (see algorithm 2).

In the next section, we prove the optimal error in $L^\infty(0,T;H^1(\Omega))$.

4. NIRB error estimate with parabolic equations

Main result. Our main result is the following theorem.

Theorem 4.1. *(NIRB error estimate for parabolic equations.) Let us consider the problem 2.1 with its exact solution $u(\mathbf{x}, t; \mu)$, and the full discretized solution $u_h^n(\mathbf{x}; \mu)$ to the problem 2.7. Let $(\Phi_i^h)_{i=1,\dots,N}$ be the L^2-orthonormalized and H^1-orthogonalized RB generated with the POD-Greedy 3 or the full Greedy algorithm 1 from the HF solutions of (2.7). We make the further assumption that the inverse inequality 2.16 is bounded on X^N where X^N stands for the continuous version of X_h^N.*

Let us consider the NIRB approximation, defined by (3.4). Then, $\forall n = 0, \dots, N_T$, the following estimate holds

$$\left|u(t^n)(\mu) - u_{Hh}^{N,n}(\mu)\right|_{H^1(\Omega)} \leq \varepsilon(N) + C_1(\mu)h + C_2(N)H^2 + C_3(\mu)\Delta t_F + C_4(N)\Delta t_G^2, \tag{4.1}$$

where C_1, C_2, C_3 and C_4 are constants independent of h and H, Δt_F and Δt_G. The term $\varepsilon(N)$ measures the error given by (1.7) and depends on the Kolmogorov N-width which shows how well the solution manifold can be approximated by N dimensional linear reduced spaces.

Remark 4.2. This theorem can be generalized to $\mathbb{P}_k$ FEM space, with $k > 1$.

Corollary 4.3 (of Theorem 4.1)**.** *Under the same assumptions than Theorem 4.1, and if H is such as $H^2 \sim h$ and $\Delta t_G^2 \sim \Delta t_F$, then (4.1) yields*

$$\forall n = 0, \dots, N_T, \ \left|u(t^n)(\mu) - u_{Hh}^{N,n}(\mu)\right|_{H^1(\Omega)} \leq \varepsilon(N) + \mathcal{O}(h + \Delta t_F), \tag{4.2}$$

if $\varepsilon(N)$ is small enough, this inequality states that we recover optimal error estimates in $L^\infty(0, T; H^1(\Omega))$.

Remark 4.4. $\varepsilon(N)$ depends on the Kolmogorov N-width, and we discuss its behaviour as a function of N in Appendix C.

With the L^2 norm, we obtain the following theorem.

Theorem 4.5. *With the same assumptions as in the Theorem 4.1, with the L^2-orthonormalized RB, the following estimate holds*

$$\forall n = 0, \dots, \frac{\Delta t_F}{T}, \ \left\|u(t^n)(\mu) - u_{Hh}^{N,n}(\mu)\right\|_{L^2(\Omega)} \leq \varepsilon'(N) + C_1'(H^2 + \Delta t_G^2) + C_2'(h^2 + \Delta t_F), \tag{4.3}$$

where C_1' and C_2' are constants independent of h, H and N, and $\varepsilon'(N)$ depends on N, and corresponds to the L^2 error between the fine solution and its projection on the reduced space of dimension N.

Remark 4.6. Note that now C_2' does not depend on N, unlike C_2 or C_4 above.

We now go on with the proof of Theorem 4.1.

Proof. The NIRB approximation at time step $n = 0, \dots, N_T$, for a new parameter $\mu \in \mathcal{G}$ is defined by (3.4). Thus, the NIRB error can be decomposed in three contributions

$$\begin{aligned}
&\left|u(t^n; \mu) - u_{Hh}^{N,n}(\mu)\right|_{H^1(\Omega)} \\
&\leq \left|u(t^n; \mu) - u_h^n(\mu)\right|_{H^1(\Omega)} + \left|u_h^n(\mu) - u_{hh}^{N,n}(\mu)\right|_{H^1(\Omega)} + \left|u_{hh}^{N,n}(\mu) - u_{Hh}^{N,n}(\mu)\right|_{H^1(\Omega)} \\
&=: T_1 + T_2 + T_3,
\end{aligned}$$

where the term

$$u_{hh}^{N,n}(\mu) := \sum_{i=1}^{N} (u_h^n(\mu), \Phi_i^h)\ \Phi_i^h, \tag{4.4}$$

is the L^2-projection of $u_h^n(\mu)$ on X_h^N.

• The first term T_1 may be estimated using the inequality (2.12), such that

$$\left|u(t^n;\mu) - u_h^n(\mu)\right|_{H^1(\Omega)} \leq C(\mu)\ (h + \Delta t_F). \tag{4.5}$$

• We denote by $\mathcal{S}_h = \{u_h^n(\mu,t), \mu \in \mathcal{G},\ n = 0,\dots N_T\}$ the set of all the solutions. For our model problem, this manifold has a low complexity. It means that

$$\left|u_h^n(\mu) - \sum_{i=1}^{N}(u_h^n(\mu),\Phi_i^h)\ \Phi_i^h\right|_{H^1(\Omega)} \leq \varepsilon(N). \tag{4.6}$$

where $\varepsilon(N)$ depends on the Kolmogorov N-width.

• For the third term T_3, let us consider the Greedy approach with a Gram–Schmidt procedure and an eigenvalue problem (3.2), which yields an orthogonalization in $L^2(\Omega)$ and in $H^1(\Omega)$. Therefore,

$$\left|u_{hh}^{N,n} - u_{Hh}^{N,n}\right|^2_{H^1(\Omega)} = \sum_{i=1}^{N}|(u_h^n(\mu) - \widetilde{u_H}^n(\mu),\Phi_i^h)|^2|\Phi_i^h|^2_{H^1(\Omega)}, \tag{4.7}$$

where $\widetilde{u_H}^n(\mu)$ is the quadratic interpolation of the coarse snapshots on time t^n, $\forall n = 0,\dots,N_T$, defined by (2.14). From the RB orthonormalization in $L_2(\Omega)$, the equation (3.2) yields

$$|\Phi_i^h|^2_{H^1} = \lambda_i \left\|\Phi_i^h\right\|^2_{L^2(\Omega)} = \lambda_i \leq \max_{j=1,\dots,N}\lambda_j = \lambda_N,$$

such that the equation (4.7) yields

$$|u_{hh}^{N,n} - u_{Hh}^{N,n}|^2_{H^1(\Omega)} \leq C\lambda_N \left\|u_h^n(\mu) - \widetilde{u_H}^n(\mu)\right\|^2_{L^2(\Omega)}. \tag{4.8}$$

Now by definition of $\widetilde{u_H}^n(\mu)$ and by Corollary 2.15 and Theorem 2.3, for $t^n \in I_m$,

$$\|u_h^n(\mu) - \widetilde{u_H}^n(\mu)\|_{L^2(\Omega)} \leq C(H^2 + \Delta t_G^2 + h + \Delta t_F),$$

and we end up for equation (4.8) with

$$|u_{hh}^{N,n} - u_{Hh}^{N,n}|_{H^1(\Omega)} \leq C\sqrt{\lambda_N}(H^2 + \Delta t_G^2 + h + \Delta t_F), \tag{4.9}$$

where C does not depend on N. Combining these estimates (4.5), (C.2) and (4.9), we obtain the estimate (4.1) and that concludes the proof. In appendix, Section C, the reader may see the values of λ_N obtained for the heat equation and for the Brusselator. ∎

We proceed with the proof of Theorem 4.5.

Proof. In analogy with the H^1 estimate, we have $\forall n = 0,\dots,N_T$,

$$\begin{aligned}
&\left\|u(t^n;\mu) - u_{Hh}^{N,n}(\mu)\right\|_{L^2(\Omega)} \\
&\leq \|u(t^n;\mu) - u_h^n(\mu)\|_{L^2(\Omega)} + \left\|u_h^n(\mu) - u_{hh}^{N,n}(\mu)\right\|_{L^2(\Omega)} + \left\|u_{hh}^{N,n}(\mu) - u_{Hh}^{N,n}(\mu)\right\|_{L^2(\Omega)} \\
&=: T_1 + T_2 + T_3.
\end{aligned}$$

• For the first term T_1, it follows from Theorem 2.3 that

$$T_1 \leq C(h^2 + \Delta t_F). \tag{4.10}$$

• As with the H^1 estimate, T_2 can be estimated with equation (4.6) and thus, for an accuracy $\varepsilon' = \varepsilon'(N) \leq \varepsilon(N)$ (where $\varepsilon(N)$ bounds the H^1 error)

$$T_2 \leq \varepsilon'. \tag{4.11}$$

• For the last term T_3, by L^2-orthonormality,

$$\begin{aligned}
\left\|u_{hh}^{N,n}(\mu) - u_{Hh}^{N,n}(\mu)\right\|^2_{L^2(\Omega)} &= \sum_{i=1}^{N}|(u_h^n(\mu) - u_H^n(\mu),\Psi_{h,i}^n)|^2 \left\|\Psi_{h,i}^n\right\|^2_{L^2(\Omega)} \\
&\leq C\left\|u_h^n(\mu) - u_H^n(\mu)\right\|^2_{L^2(\Omega)}.
\end{aligned}$$

Note that, the dependence in N is removed in the previous inequality. By Theorem 2.13 and triangle inequality, it leads to

$$\left\|u_{hh}^{N,n}(\mu) - u_{Hh}^{N,n}(\mu)\right\|_{L^2(\Omega)} \leq C\ (H^2 + \Delta t_G^2 + h^2 + \Delta t_F). \tag{4.12}$$

Combining (4.10), (4.11), and (4.12) concludes the proof. ∎

5. Numerical results

In this section, we have applied the NIRB algorithm on several numerical tests. For each case, we compare the plain NIRB errors (without the rectification post-treatment) with the rectified NIRB errors given by algorithm 2:

- first, on the heat equation (2.1) with $\Delta t_G \simeq H \simeq 2\ h \simeq 2\ \Delta t_F$. Note that in some situations, because of the constants C_2 and C_4 in the estimate of Theorem 4.1, the best size for the coarse mesh may not be $\Delta t_F^{1/2}$.
- then, on the heat equation with $\Delta t_G^2 \simeq H \simeq \sqrt{h} \simeq \Delta t_F$.
- finally, we also tested our problem on a more complex problem, the Brusselator system.

We have implemented both schemes (Euler and Crank–Nicolson) using FreeFem++ (version 4.9) [23] to compute the fine and coarse snapshots, and the solutions have been stored in VTK format. Then we have applied the plain NIRB and the NIRB rectified algorithm with python, in order to highlight the non-intrusive side of this method (as in [16]). After saving the NIRB approximations with Paraview module on Python, the errors have been computed with FreeFem++. These tests are available on GitHub `https://github.com/grosjean1/parabolic`, and the NIRB method is also available on Feel++[31].

5.1. The heat equation with $\Delta t_G \simeq H \simeq 2\ h \simeq 2\ \Delta t_F$

5.1.1. *Convergence results*

We have taken the parameter set $\mathcal{G} = [0.5, 9.5]$.

Note that for $\mu = 1$, we can calculate an analytical solution, which is given by

$$u(t, \mathbf{x}; 1) = 10(t+1)x^2(1-x)^2y^2(1-y)^2, \tag{5.1}$$

for a right-hand side function

$$f(t, \mathbf{x}) = 10[x^2(x-1)^2y^2(y-1)^2 - 2(t+1)((6x^2-6x+1)(y^2(y-1)^2) + (6y^2-6y+1)(x^2(x-1)^2))],$$

where $\mathbf{x} = (x, y)$. The initial solutions solve the elliptic equation (with homogeneous Dirichlet boundary conditions)

$$-\mu\Delta u_0 = f_0, \text{ with } f_0(x) = -20[(6x^2-6x+1)(y^2(y-1)^2) + (6y^2-6y+1)(x^2(x-1)^2)].$$

As a result, we have employed for $\mu = 1$ the Ritz projection (2.5) to compute the initial solution u_h^0 with $u^0 = u(0, \mathbf{x}; 1)$ as in (2.6).

We have retrieved several snapshots on $t = [0, 1]$ (note that the coarse time grid must belong to the interval of the fine one), and tried our algorithms on several size of meshes, always with $\Delta t_F \simeq h$ and $\Delta t_G \simeq H$ (both schemes are stable).

We have first taken 18 parameters in $\mathcal{G}$ for the RB construction such that $\mu_i = 0.5i,\ i = 1, \dots, 19,\ i \neq 2$, and the true solution (5.1), with $\mu = 1$. In 5.1 and 5.2, we present the errors of the FEM solutions and compare them to the ones obtained with the NIRB algorithms with $N = 5$ to observe the convergence rates.

We recall that the rectification post-processing step is done for each time step and that the corresponding NIRB method is given by (3.5), where the rectification matrix R may be seen as a family of 2nd-order tensors indexed by n.

The NIRB error in the $l^\infty(0, \dots, N_T;\ H_0^1(\Omega))$ norm is defined as

$$\frac{\left\| u(1) - u_{Hh}^N(1) \right\|_{l^\infty(0,\dots,N_T;\ H_0^1(\Omega))}}{\|u(1)\|_{l^\infty(0,\dots,N_T;\ H_0^1(\Omega))}}, \tag{5.2}$$

and with the rectification post-treatment we have

$$\frac{\left\| u(1) - R[u_{Hh}^N](1) \right\|_{l^\infty(0,\dots,N_T;\ H_0^1(\Omega))}}{\|u(1)\|_{l^\infty(0,\dots,N_T;\ H_0^1(\Omega))}}, \tag{5.3}$$

where $R[u_{Hh}^N]$ is defined by (3.5), and these relative errors are compared to the FEM ones defined (resp. for fine solutions and coarse ones) as

$$\frac{\|u(1) - u_h(1)\|_{l^\infty(0,\dots,N_T;\ H_0^1(\Omega))}}{\|u(1)\|_{l^\infty(0,\dots,N_T;\ H_0^1(\Omega))}} \quad \text{and} \quad \frac{\|u(1) - u_H(1)\|_{l^\infty(0,\dots,M_T;\ H_0^1(\Omega))}}{\|u(1)\|_{l^\infty(0,\dots,M_T;\ H_0^1(\Omega))}}. \tag{5.4}$$

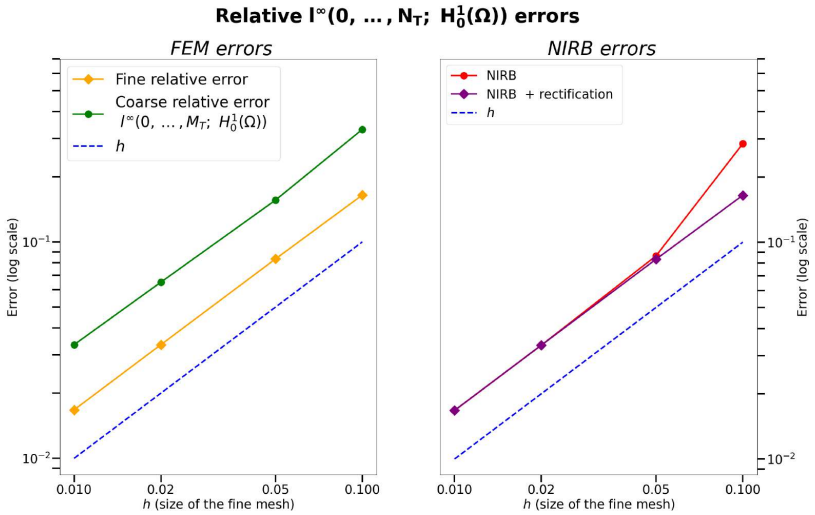

Figure 5.1. $\Delta t_G \simeq H \simeq 2\ h \simeq 2\ \Delta t_F$. Convergence rate for $\mu = 1$ (as a new parameter): FEM $L^\infty(0, \dots, N_T;\ H_0^1(\Omega))$ (fine) and $L^\infty(0, \dots, M_T;\ H_0^1\Omega))$ (coarse) relative errors (5.4) for several sizes of mesh (left) compared to the NIRB method with $(N = 5)$ and without the rectification post-treatment $(N = 5)$ (right) (5.3)

We plot the $l^\infty(0, \dots, N_T;\ L^2(\Omega))$ relative errors in Figure 5.2.

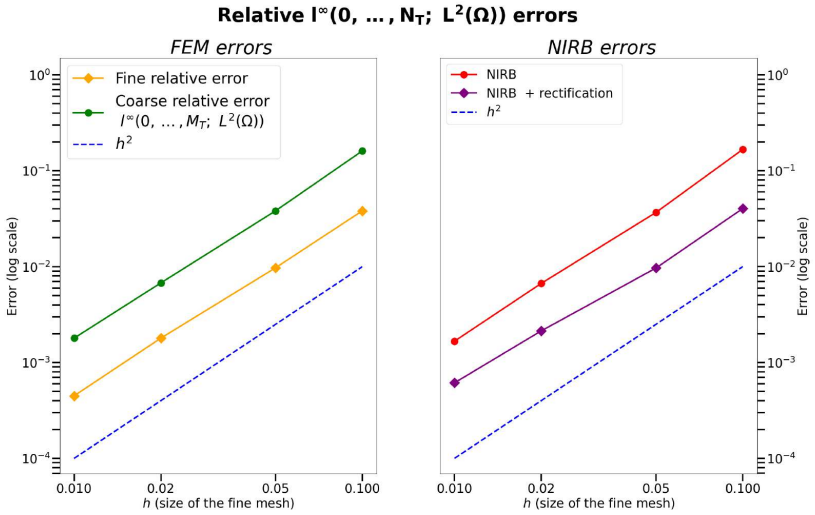

FIGURE 5.2. $\Delta t_G \simeq H \simeq 2\ h \simeq 2\ \Delta t_F$. Convergence rate for $\mu = 1$ (as a new parameter): FEM $L^\infty(0,\dots,N_T;\ L^2(\Omega))$ (fine) and $L^\infty(0,\dots,M_T;\ L^2\Omega))$ (coarse) relative errors (5.4) for several sizes of mesh (left) compared to the NIRB method with ($N = 5$) and without the rectification post-treatment ($N = 5$) (right)

TABLE 5.1. Relative errors in $l^\infty(0,\dots,N_T;\ H_0^1(\Omega))$ over the parameters (NIRB errors with $H \simeq 2h$ compared to the true RB projection (4.4) and to the FEM fine and coarse projection) with $N = 5$ with $h = 0.01$

NIRB rectified error $\max_{\mu\in\mathcal{G}_{\text{train}}\setminus\{0.5,9.5\}} \frac{\left\|u_{ref}(\mu)-R[u^N_{Hh}](\mu)\right\|_{l^\infty(0,\dots,N_T;\ H_0^1(\Omega))}}{\left\|u_{ref}(\mu)\right\|_{l^\infty(0,\dots,N_T;\ H_0^1(\Omega))}}$	1.63620×10^{-2}
NIRB error (without rectification) $\max_{\mu\in\mathcal{G}_{\text{train}}\setminus\{0.5,9.5\}} \frac{\left\|u_{ref}(\mu)-u^N_{Hh}(\mu)\right\|_{l^\infty(0,\dots,N_T;\ H_0^1(\Omega))}}{\left\|u_{ref}(\mu)\right\|_{l^\infty(0,\dots,N_T;\ H_0^1(\Omega))}}$	1.65037×10^{-2}
RB projection $\max_{\mu\in\mathcal{G}_{\text{train}}\setminus\{0.5,9.5\}} \frac{\left\|u_{ref}(\mu)-u^N_{hh}(\mu)\right\|_{l^\infty(0,\dots,N_T;\ H_0^1(\Omega))}}{\left\|u_{ref}(\mu)\right\|_{l^\infty(0,\dots,N_T;\ H_0^1(\Omega))}}$	1.63617×10^{-2}
Fine FEM projection $\max_{\mu\in\mathcal{G}_{\text{train}}\setminus\{0.5,9.5\}} \frac{\left\|u_{ref}(\mu)-u_h(\mu)\right\|_{l^\infty(0,\dots,N_T;\ H_0^1(\Omega))}}{\left\|u_{ref}(\mu)\right\|_{l^\infty(0,\dots,N_T;\ H_0^1(\Omega))}}$	1.63617×10^{-2}
Coarse FEM projection $\max_{\mu\in\mathcal{G}_{\text{train}}\setminus\{0.5,9.5\}} \frac{\left\|u_{ref}(\mu)-u_H(\mu)\right\|_{l^\infty(0,\dots,M_T;\ H_0^1(\Omega))}}{\left\|u_{ref}(\mu)\right\|_{l^\infty(0,\dots,M_T;\ H_0^1(\Omega))}}$	3.58067×10^{-2}

Then, we have taken 19 parameters in $\mathcal{G}$ for the RB construction such that $\mu_i = 0.5i,\ i = 1,\dots,19$ and have applied the "leave-one-out" strategy. It involves removing each training test parameter from the RB in order to obtain its associated NIRB approximation. It allows us to evaluate the NIRB algorithm with respect to the parameters. Table 5.1 presents the maximum $l^\infty(0,\dots,N_T;\ H_0^1(\Omega))$-error of the NIRB approximations over the parameters. To represent the true solution, we have computed a $\mathbb{P}_1$ reference approximation $u_{ref}(\mu)$ on a finer mesh with $h_{ref} \simeq \Delta t_{ref} = 0.0025$. We have excluded 0.5 and 9.5 to not extrapolate over the parameters.

5.1.2. *Time execution (min,sec)*

We present the FEM and NIRB run-times in Table 5.2.

Table 5.2. FEM and NIRB run-times ($N = 10$)

FEM high fidelity solver	FEM coarse solution
00:03	00:02
NIRB Offline	Rectified NIRB online
1:45	00:02

5.2. **The heat equation with** $H^2 \simeq h \simeq \Delta t_G^2 \simeq \Delta t_F$

5.2.1. *Convergence results*

As previously, we display the convergence rate of the FEM approximations (left) and of the NIRB approximations (with and without rectification and with $N = 5$) in Figure 5.3. For all meshes, we choose $\mu = 1$ and as expected, we observe that both NIRB $l^\infty(1, \dots, N_T; H_0^1(\Omega))$ errors converge in $\mathcal{O}(h + \Delta t_F)$, and we retrieve the HF accuracy with the rectified NIRB approximation.

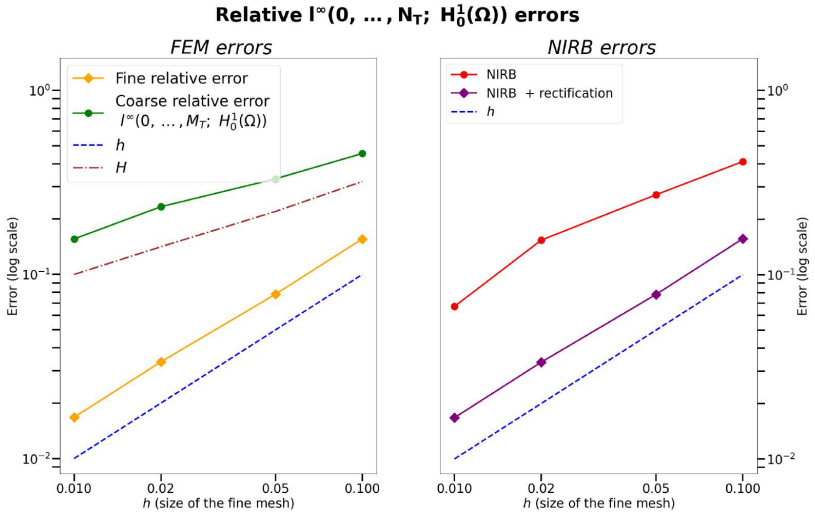

Figure 5.3. $H^2 \simeq h \simeq \Delta t_G^2 \simeq \Delta t_F$. Convergence rate for $\mu = 1$ (as a new parameter): FEM $L^\infty(0, \dots, N_T;\ H_0^1(\Omega))$ (fine) and $L^\infty(0, \dots, M_T;\ H_0^1\Omega))$ (coarse) relative errors (5.4) for several sizes of mesh (left) compared to the NIRB method with $(N = 5)$ and without the rectification post-treatment $(N = 5)$ (right) (5.3)

We also plot the $l^\infty(1, \dots, N_T; L^2(\Omega))$ errors in Figure 5.4. Finally, in order to evaluate the NIRB algorithm with respect to the parameters, Table 5.3 presents the maximum $l^\infty(1, \dots, N_T; H_0^1(\Omega))$-error of the approximations over the parameters.

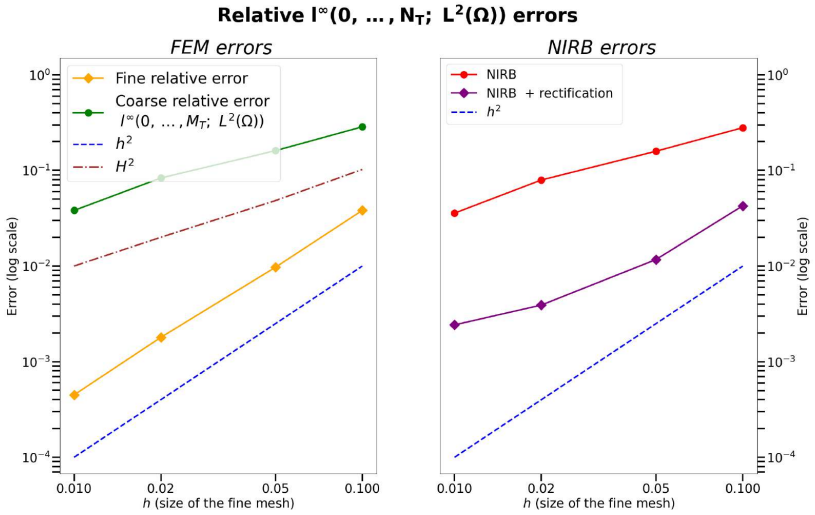

FIGURE 5.4. $H^2 \simeq h \simeq \Delta t_G^2 \simeq \Delta t_F$. Convergence rate for $\mu = 1$ (as a new parameter): FEM $L^\infty(0,\dots,N_T;\ L^2(\Omega))$ (fine) and $L^\infty(0,\dots,M_T;\ H_0^1\Omega))$ (coarse) relative errors (5.4) for several sizes of mesh (left) compared to the NIRB method with ($N = 5$) and without the rectification post-treatment ($N = 5$) (right) (5.3)

TABLE 5.3. Relative $l^\infty(0,\dots,N_T;\ H_0^1(\Omega))$ errors over the parameters (NIRB errors with $H \simeq h^{1/2}$ compared to the true RB projection (4.4) and to the FEM fine and coarse projection) with $N = 5$ with $h = 0.01$

NIRB rectified error	$\max_{\mu\in\mathcal{G}_{\text{train}}\setminus\{0.5,9.5\}} \frac{\left\|u_{ref}(\mu)-R[u_{Hh}^N](\mu)\right\|_{l^\infty(0,\dots,N_T;\ H_0^1(\Omega))}}{\left\|u_{ref}(\mu)\right\|_{l^\infty(0,\dots,N_T;\ H_0^1(\Omega))}}$	1.63620×10^{-2}
NIRB error (without rectification)	$\max_{\mu\in\mathcal{G}_{\text{train}}\setminus\{0.5,9.5\}} \frac{\left\|u_{ref}(\mu)-u_{Hh}^N(\mu)\right\|_{l^\infty(0,\dots,N_T;\ H_0^1(\Omega))}}{\left\|u_{ref}(\mu)\right\|_{l^\infty(0,\dots,N_T;\ H_0^1(\Omega))}}$	6.23300×10^{-2}
RB projection	$\max_{\mu\in\mathcal{G}_{\text{train}}\setminus\{0.5,9.5\}} \frac{\left\|u_{ref}(\mu)-u_{hh}^N(\mu)\right\|_{l^\infty(0,\dots,N_T;\ H_0^1(\Omega))}}{\left\|u_{ref}(\mu)\right\|_{l^\infty(0,\dots,N_T;\ H_0^1(\Omega))}}$	1.63617×10^{-2}
Fine FEM projection	$\max_{\mu\in\mathcal{G}_{\text{train}}\setminus\{0.5,9.5\}} \frac{\left\|u_{ref}(\mu)-u_h(\mu)\right\|_{l^\infty(0,\dots,N_T;\ H_0^1(\Omega))}}{\left\|u_{ref}(\mu)\right\|_{l^\infty(0,\dots,N_T;\ H_0^1(\Omega))}}$	1.63617×10^{-2}
Coarse FEM projection	$\max_{\mu\in\mathcal{G}_{\text{train}}\setminus\{0.5,9.5\}} \frac{\left\|u_{ref}(\mu)-u_H(\mu)\right\|_{l^\infty(0,\dots,M_T;\ H_0^1(\Omega))}}{\left\|u_{ref}(\mu)\right\|_{l^\infty(0,\dots,M_T;\ H_0^1(\Omega))}}$	1.55981×10^{-1}

In Figure 5.5, the maximum $H_0^1(\Omega)$ errors are displayed for $\mu = 1$ and different number of modes N, and we observe that the errors without the rectification post-treatment increases with N due to the role of the constants C_2 and C_4 in the estimate of Theorem 4.1, whereas with the post-treatment they remain stable.

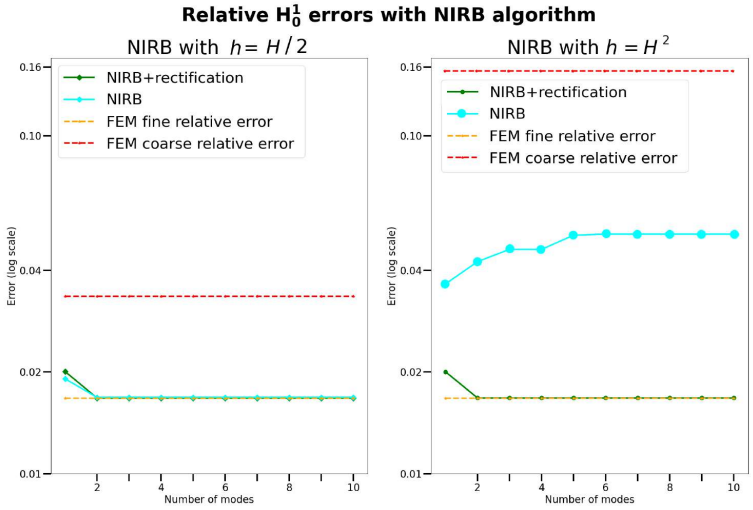

FIGURE 5.5. For $h = 0.01$: $H = 2h$ (left), $h = H^2$ (right) $\mu = 1$, NIRB relative H_0^1 errors and rectified NIRB (+ rectification post-treatment) H_0^1 compared to FEM errors with different modes N

Remark 5.1. We may also consider NIRB aproximations of (2.7) under the form

$$u_{Hh}^{N,n}(\mathbf{x};\mu) = \sum_{i=1}^{N} \alpha_i^H(\mu, t^n)\ \Phi_{h,i}^n(\mathbf{x}),\ n \geq 0, \tag{5.5}$$

with $(\Phi_{h,i}^n)_{i=1,\dots,N}$ time-dependent basis functions. This time, the Greedy algorithm 1 is executed for each time step and thus, this method is less efficient (in term of storage) since we have to store N times the number of time steps of the reduced basis.

With this decomposition, we obtained the following results (see Figure 5.6).

5.2.2. *Time execution (min,sec)*

We present the FEM and NIRB run-times in Table 5.4.

TABLE 5.4. FEM and NIRB run-times ($N = 10$)

FEM high fidelity solver	FEM coarse solution
00:03	00:01
NIRB Offline	classical rectified NIRB online
1:32	00:02

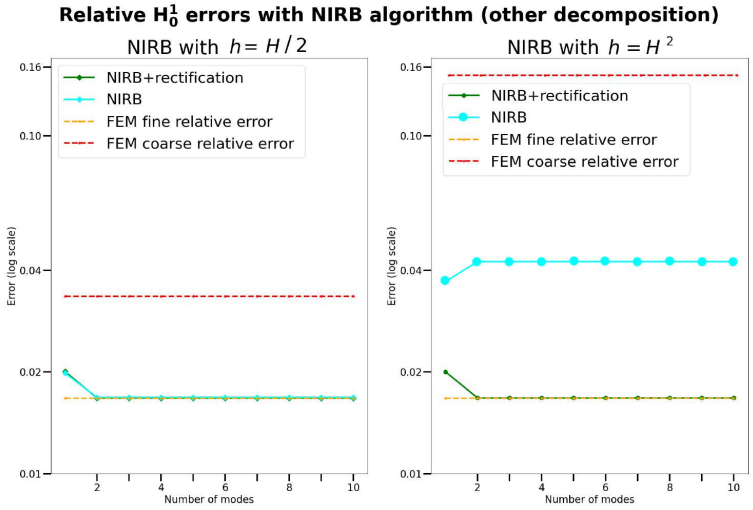

FIGURE 5.6. For $h = 0.01$: $H = 2h$ (left), $h = H^2$ (right) $\mu = 1$, NIRB relative H_0^1 errors and rectified NIRB (+ rectification post-treatment) H_0^1 compared to FEM errors with different modes N *using the other NIRB decomposition* (5.5)

5.3. **Comments on the results**

- On the first tests, with $\Delta t_G \simeq H \simeq 2\ h \simeq 2\ \Delta t_F$, we observe the following facts:
  - with and without the rectification post-treatment, the method converges in $\mathcal{O}(h + \Delta t_F)$, as expected from the estimates of Theorem 4.1 for the plain NIRB (see Figure 5.1).
  - we obtain the same accuracy as with the HF solutions in the H_0^1 norm in both cases.
  - we find an optimal L^2 error estimate for the NIRB with the rectification post-treatment, in $\mathcal{O}(h^2 + \Delta t_F)$, whereas the error for the plain NIRB is not enhanced by the NIRB algorithm (compared to the coarse FEM approximation), as predicted by Theorem 4.5 (see Figure 5.2).

  The rough mesh size is finer than $\sqrt{h}$. In that case, the plain NIRB algorithm is sufficient to retrieve the optimal H^1 accuracy.

- Then, on the heat equation with $\Delta t_G^2 \simeq H \simeq \sqrt{h} \simeq \Delta t_F$, we remark that
  - with both algorithms, the error converge in $\mathcal{O}(h + \Delta t_F)$ (see Figure 5.3).
  - The plain NIRB method allows us to reduce the H_0^1 error compared to the coarse FEM approximation. Yet, the fine accuracy is recovered only while adding the rectification post-treatment.
  - We retrieved the rates of convergence expected from Theorem 4.5 in $\mathcal{O}(h^2 + \Delta t_F)$, yet only the NIRB with the rectification post-treatment yields an accuracy very close to the HF ones (see Figure 5.4).

Table 5.5. Relative $l^\infty(0,\dots,N_T;\ H^1(\Omega))$ errors (and $l^\infty(0,\dots,M_T;\ H^1(\Omega))$ for the coarse ones) with leave-one-out strategy $N = 30$

Parameters a-b-α	Fine error	Coarse error	True projection u_{hh}^N	NIRB + rectification	classical NIRB
3-2-0.002	4.54×10^{-2}	1.70×10^{-1}	4.56×10^{-2}	5.07×10^{-2}	1.54×10^{-1}
4-2-0.01	3.54×10^{-2}	1.75×10^{-1}	3.79×10^{-2}	6.01×10^{-2}	1.30×10^{-1}
4-3-0.005	3.80×10^{-2}	1.86×10^{-1}	3.80×10^{-2}	3.97×10^{-2}	1.69×10^{-1}
4-4-0.0002	5.04×10^{-2}	8.56×10^{-2}	5.04×10^{-2}	5.04×10^{-2}	8.90×10^{-2}
5-2-0.001	4.84×10^{-2}	1.72×10^{-1}	4.83×10^{-2}	6.24×10^{-2}	1.66×10^{-1}
5-3-0.008	3.61×10^{-2}	1.73×10^{-1}	3.61×10^{-2}	3.61×10^{-2}	1.71×10^{-1}

5.4. **The parameterized Brusselator equations**

The Brusselator problem [30] involves chemical reactions. It is a more complex test from a simulation point of view. The chemical concentrations in this problem are controlled by parameters throughout the reaction process, making it an interesting application of a NIRB method. Let us introduce the Brusselator problem in a spatial domain $\Omega = [0,1]^2$. The nonlinear system of this two-dimensional reaction-diffusion problem writes

$$\begin{cases} \partial_t u_1 = a + u_1 u_2^2 - (b+1)u_1 + \alpha \Delta u_1, & \text{in } \Omega \times]0,T] \\ \partial_t u_2 = b u_1 - u_1\ u_2^2 + \alpha \Delta u_2, & \text{in } \Omega \times]0,T], \\ u_1(\mathbf{x},0) = u^0(\mathbf{x}) = 2 + 0.25y, & \text{in } \Omega \\ u_2(\mathbf{x},0) = v_0(\mathbf{x}) = 1 + 0.8x, & \text{in } \Omega, \\ \partial_n u_1 = 0, & \partial\Omega, \\ \partial_n u_2 = 0, & \partial\Omega. \end{cases} \tag{5.6}$$

We now have to deal with a nonlinearity as well as two unknowns. Our parameter, denoted $\boldsymbol{\mu} = (a, b, \alpha)$, belongs to $[2,6] \times [1,8] \times [0.0001, 0.05]$. We have taken an ending time $T = 5$. These parameters are standard [30] and we note that, for $b \leq 1 + a^2$, the solutions are global, and for α small enough, they converge to $(u_l, v_l) = (a, \frac{b}{a})$.

We use an Euler implicit scheme for fine solutions with the Newton algorithm to deal with the nonlinearity and a Runge–Kutta 2 (RK2) scheme for the coarse mesh. Indeed, solutions blow up with an explicit Euler scheme, whereas they remain stable for our parameters with an order 2 scheme.

We have randomly chosen 8 training parameters and have applied a "leave-one-out" strategy (we have excluded from the tested parameters the set extremities). A sign of a good reduced basis is the estimation of a small Kolmogorov N-width by rapid decay of projection errors of these training solutions onto the N-dimensional RB space. In figure 5.7, we see the maximal relative projection errors in $l^\infty(0,\dots,N_T;\ H^1(\Omega))$ norm as a function of N.

We have employed a refined mesh to represent the solution of reference (with $h_{ref} = \Delta t_{ref} = 0.005$). In Table 5.5, we have compared the $l^\infty(0,\dots,N_T;\ H^1(\Omega))$ error of the fine FEM solutions to the corresponding NIRB errors with and without the rectification post-treatment with $N = 30$ modes with $h = 0.02 = \Delta t_F \simeq H^2 = \Delta t_G^2$ ($\Delta T_G = H = 0.2$). In order to then observe the effect of the number of modes N on the NIRB approximation, we plot the errors of the NIRB approximation with and without the rectification post-treatment and of the FEM fine and coarse approximations in Figure 5.7 and compare the errors to the true projection for the worst-case scenario (with $a = 4$, $b = 2$ and $\alpha = 0.01$).

In 5.8 follows the NIRB rectified solution for $N = 10$ modes at time $T = 5$ for the two variables u_1 and u_2 with the parameter $(a, b, \alpha) = (3, 2, 0.002)$. The approximation is close to $(a, \frac{b}{a}) = (3, 2/3)$ as expected.

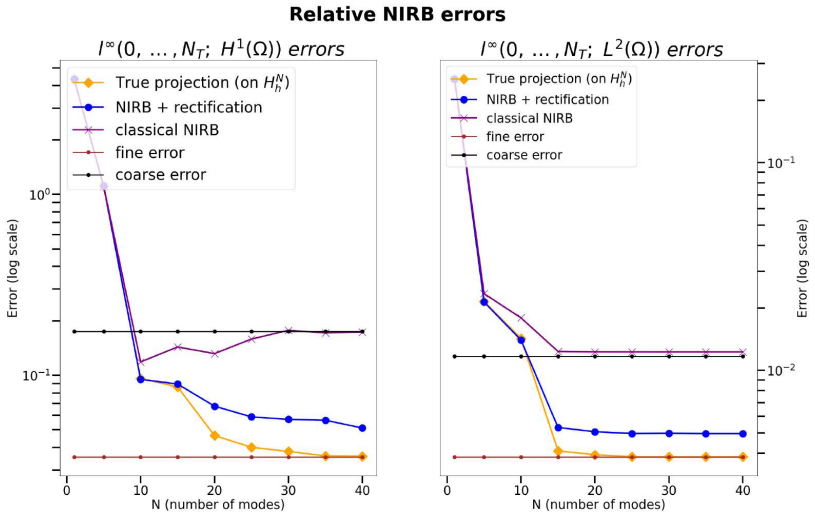

FIGURE 5.7. Worst-case scenario: test with $l^\infty(0,\dots,N_T;H^1(\Omega))$ relative errors with a new parameter $(a,b,\alpha)=(4,2,0.01)$, $t_0=0$, $T=5$, $\Omega=[0,1]\times[0,1]$ (NIRB errors compared to fine and coarse FEM errors)

(A) u_1 (B) u_2

FIGURE 5.8. NIRB rectified approximations (u_1 (left) and u_2 (right)) for $T=5$ with $N=10$ modes (close to $(a,\frac{b}{a})=(3,2/3)$)

5.4.1. *Time execution (min,sec)*

Finally, the computational costs are significantly reduced during the online part of the algorithm as highlighted by this example. Indeed, since there is a nonlinearity, the system must be solved with several iterations for each time step, and thus is quite expensive for a HF approximation. We recall that with an explicit Euler scheme, the solution blows up whereas with the RK2 scheme (without iteration), the solution converges to the expected values $(a,\frac{b}{a})$.

We present the FEM and NIRB run-times in Table 5.6.

Table 5.6. FEM and NIRB run-times ($N = 10$, h:min:sec)

FEM high fidelity solver	FEM coarse solution
00:04:52	00:00:02
NIRB Offline	classical rectified NIRB online
01:53:00	00:00:04

6. Conclusion

In this paper, we extend the NIRB 2-grid method to parabolic equations. For this purpose, the offline part of the algorithm is modified allowing a compression of the solutions in both directions of parameters and time. The RB functions are time independent and the NIRB accuracy is improved by a time-dependent rectification post-treatment described in Section 3.

In Section 4, we prove that we recover optimal estimates for the NIRB approximations in $L^\infty(0,T;H^1(\Omega))$ on a model problem, which is the heat equation. Our main result is given by Theorem 4.1 which announces the precise $L^\infty(0,T;H^1(\Omega))$ error estimate. We also prove an $L^\infty(0,T;L^2(\Omega))$ estimate.

Finally, we present in Section 5 several numerical results on the heat equation and on the Brusselator problem, that are consistent with the theory. On the heat equation, we have tested the method with several grid sizes: $\Delta t_G \simeq H \simeq 2\ h \simeq 2\ \Delta t_F$ and then with $\Delta t_G^2 \simeq H \simeq \sqrt{h} \simeq \Delta t_F$. We observe, as described in Section 5.3, that the HF accuracy is recovered with the rectification post-treatment in both cases, in the $L^\infty(0,T;H^1(\Omega))$ norm. Without this post-treatment, the NIRB method reduces the error and retrieves the fine accuracy in the first case. The optimal convergence rates are recovered in both cases. We also illustrate the method with several results on the $L^2(\Omega)$ norm and demonstrate its efficiency to retrieve the HF accuracy with the rectification post-treatment.

The brusselator problem is more complex than the heat equation from a simulation standpoint. As a matter of fact, we observe that more RB functions are required to retrieve the fine precision (see Figure 5.7). Yet, we still observe very good results as presented in Table 5.5 thanks to the rectification post-treatment. Indeed, with a leave-one-out strategy, we observe with $\Delta t_G^2 \simeq H \simeq \sqrt{h} \simeq \Delta t_F$ that it yields the fine accuracy in almost all cases presented in table 5.5 and that the NIRB error with this post-treatment is very close to the fine error in the worst-case scenario.These tests highlight the great capability of this method in reducing simulation costs: run-times are indeed significantly reduced compared to an HF evaluation, as observed in Table 5.6.

Appendix A. POD-Greedy algorithm

Algorithm 3 POD-Greedy algorithm

Input: N_{max}, $\{u_h^n(\mu_1), \dots, u_h^n(\mu_{N_{\text{train}}})$ with $\mu_i \in \mathcal{G}_{\text{train}},\ n = 0, \dots, N_T\}$.
Output: Reduced basis $\{\Phi_1^h, \dots, \Phi_N^h\}, N \leq N_{max}$.

Choose $\mu_1 = \text{argmax}_{\mu \in \mathcal{G}_{\text{train}}} \|u_h(\mu)\|_{l^\infty(0,\dots,N_T;\ L^2(\Omega))}$.
Then produce the modes $\{\Phi_1^h, \dots, \Phi_{N_1}^h\}$ through a POD on $\{u_h^n(\mu_1),\ n = 0, \dots, N_T\}$.
Set $\mathcal{G}_1 = \mu_1$ and $X_h^1 = \text{span}\{\Phi_1^h, \dots, \Phi_{N_1}^h\}$.
while $\sum_{k=2}^{N} N_k < N_{max}$ **do**
  Choose $\mu_k = \text{argmax}_{\mu \in \mathcal{G}_{\text{train}} \setminus \mathcal{G}_{k-1}} \frac{\left\|u_h(\mu) - P^{k-1}(u_h(\mu))\right\|_{l^\infty(0,\dots,N_T;L^2(\Omega))}}{\|u_h(\mu)\|_{l^\infty(0,\dots,N_T;L^2(\Omega))}}$,
    with $P^{k-1}(u_h(\mu)) := \sum_{i=1}^{N_{k-1}} (u_h(\mu), \Phi_i^h)_{L^2} \Phi_i^h$.
  Then produce the modes $\{\Phi_{N_{k-1}+1}^h, \dots, \Phi_{N_k}^h\}$ through a POD on
    $\{u_h^n(\mu_k) - P^{k-1}(u_h^n(\mu_k)),\ n = 0, \dots, N_T\}$.
  Set $\mathcal{G}_k = \mathcal{G}_{k-1} \cup \mu_k$ and $X_h^k = X_h^{k-1} \oplus \text{span}\{\Phi_{k-1}^h, \dots, \Phi_{N_k}^h\}$.
end while

Appendix B. Proof of Theorem 2.5

Proof. We first decompose the error with two components θ and ρ such that

$$\begin{aligned} \forall n = 1, \dots N_T,\ e^n &:= \sqrt{\mu}(\nabla u_h^n - \nabla u(t^n)) = \sqrt{\mu}((\nabla u_h^n - \nabla P_h^1 u(t^n)) + (\nabla P_h^1 u(t^n) - \nabla u(t^n))), \\ &= \sqrt{\mu}(\nabla \theta^n + \nabla \rho^n). \end{aligned} \tag{B.1}$$

• For the estimate on ρ^n, a classical FEM estimate [3, 34] is

$$\left\|P_h^1 v - v\right\|_{L^2(\Omega)} + h \left\|\nabla(P_h^1 v - v)\right\|_{L^2(\Omega)} \leq Ch^2 \|v\|_{H^2(\Omega)}, \quad \forall v \in H^2 \cap H_0^1,$$

which leads to

$$\|\nabla \rho^n\|_{L^2(\Omega)} \leq Ch \|u(t^n)\|_{H^2(\Omega)},\ \forall n = 0, \dots N_T,$$

and then to

$$\|\nabla \rho^n\|_{L^2(\Omega)} \leq Ch \left[\left\|u^0\right\|_{H^2(\Omega)} + \int_0^{t^n} \|u_t\|_{H^2(\Omega)}\ ds\right]. \tag{B.2}$$

• For the estimate on θ, let us consider $v \in V_h$. Since the operators P_h^1 and $\overline{\partial}$ commute, we may write

$$(\overline{\partial}\theta^n, v) + \mu(\nabla \theta^n, \nabla v) = (\overline{\partial} u_h^n, v) - (P_h^1 \overline{\partial} u(t^n), v) + \mu(\nabla u_h^n, \nabla v) - \mu(\nabla P_h^1 u(t^n), \nabla v).$$

The weak formulations (2.2) and (2.7) (fully-discretized solution with the Euler scheme) imply

$$\begin{aligned} (\overline{\partial}\theta^n, v) + \mu(\nabla \theta^n, \nabla v) &= (f, v) - (P_h^1 \overline{\partial} u(t^n), v) - \mu(\nabla P_h^1 u(t^n), \nabla v), \\ &= (f, v) - (P_h^1 \overline{\partial} u(t^n), v) - \mu(\nabla u(t^n), \nabla v), \text{ by definition of } P_h^1, \\ &= (u_t(t^n), v) - (P_h^1 \overline{\partial} u(t^n), v). \end{aligned}$$

Then, with the triangle inequality, it yields

$$\begin{aligned} (\overline{\partial}\theta^n, v) + \mu(\nabla \theta^n, \nabla v) &= -((P_h^1 - I)\overline{\partial} u(t^n), v) - ((\overline{\partial} u(t^n) - u_t(t^n)), v) \\ &:= -(w_1^n + w_2^n, v) = -(w^n, v). \end{aligned} \tag{B.3}$$

Instead of replacing v by θ^n as in the L^2 estimate, here we replace v by $\overline{\partial}\theta^n$, thus the equation (B.3) takes the form

$$(\overline{\partial}\theta^n, \overline{\partial}\theta^n) + \mu(\nabla \theta^n, \overline{\partial} \nabla \theta^n) = -(w^n, \overline{\partial}\theta^n).$$

Therefore, by definition of $\overline{\partial}$ for the Backward Euler discretization,

$$\underbrace{(\overline{\partial}\theta^n, \overline{\partial}\theta^n) + \mu\frac{\|\nabla\theta^n\|^2_{L^2(\Omega)}}{\Delta t_F} - \mu\frac{(\nabla\theta^n, \nabla\theta^{n-1})}{\Delta t_F}}_{T_a} = -(w^n, \overline{\partial}\theta^n).$$

Young's inequality yields

$$(\nabla\theta^n, \nabla\theta^{n-1}) \leq \frac{1}{2}\|\nabla\theta^n\|^2_{L^2(\Omega)} + \frac{1}{2}\left\|\nabla\theta^{n-1}\right\|^2_{L^2(\Omega)},$$

therefore

$$\left\|\overline{\partial}\theta^n\right\|^2_{L^2(\Omega)} + \mu\frac{\|\nabla\theta^n\|^2_{L^2(\Omega)}}{2\Delta t_F} - \mu\frac{\left\|\nabla\theta^{n-1}\right\|^2_{L^2(\Omega)}}{2\Delta t_F} \;\leq\; T_a \;\leq\; \frac{1}{2}\|w^n\|^2_{L^2(\Omega)} + \frac{1}{2}\left\|\overline{\partial}\theta^n\right\|^2_{L^2(\Omega)},$$

and it results in

$$\left\|\overline{\partial}\theta^n\right\|^2_{L^2(\Omega)} + \mu\frac{\|\nabla\theta^n\|^2_{L^2(\Omega)}}{\Delta t_F} \leq \mu\frac{\left\|\nabla\theta^{n-1}\right\|^2_{L^2(\Omega)}}{\Delta t_F} + \|w^n\|^2_{L^2(\Omega)}.$$

Since $\left\|\overline{\partial}\theta^n\right\|^2_{L^2(\Omega)} \geq 0$, it follows that

$$\forall n = 1, \ldots, N_T,\ \|\nabla\theta^n\|^2_{L^2(\Omega)} \leq \left\|\nabla\theta^{n-1}\right\|^2_{L^2(\Omega)} + \frac{\Delta t_F}{\mu}\|w^n\|^2_{L^2(\Omega)},$$

and we recursively obtain

$$\forall n = 1, \ldots, N_T,\ \|\nabla\theta^n\|^2_{L^2(\Omega)} \leq \left\|\nabla\theta^0\right\|^2_{L^2(\Omega)} + \frac{\Delta t_F}{\mu}\sum_{j=1}^{n}\left\|w^j\right\|^2_{L^2(\Omega)}.$$

By definition of θ (and P_h^1),

$$\begin{aligned}\left\|\nabla\theta^0\right\|_{L^2(\Omega)} &= \left\|\nabla u_h^0 - \nabla P_h^1(u^0)\right\|_{L^2(\Omega)} \leq \left\|\nabla u_h^0 - \nabla u(t^0)\right\|_{L^2(\Omega)} + \left\|\nabla u^0 - \nabla P_h^1(u^0)\right\|_{L^2(\Omega)} \\ &\leq \left\|\nabla u_h^0 - \nabla u^0\right\|_{L^2(\Omega)} + Ch\left\|u^0\right\|_{H^2(\Omega)}.\end{aligned}$$

It remains to estimate the L^2 norm of the w^j, defined by (B.3).

– Let us first consider the construction for w_1

$$\begin{aligned}w_1^j &= (P_h^1 - I)\overline{\partial}u(t^j) \\ &= \frac{1}{\Delta t_F}(P_h^1 - I)\int_{t^{j-1}}^{t^j} u_t\ ds, \\ &= \frac{1}{\Delta t_F}\int_{t^{j-1}}^{t^j}(P_h^1 - I)u_t\ ds, \text{ since } P_h^1 \text{ and the time integral commute.}\end{aligned}$$

Thus, from Hölder's inequality,

$$\begin{aligned}\frac{\Delta t_F}{\mu}\sum_{j=1}^{n}\left\|w_1^j\right\|^2_{L^2(\Omega)} &\leq \frac{\Delta t_F}{\mu}\sum_{j=1}^{n}\int_\Omega\Big[\frac{1}{\Delta t_F^2}\int_{t^{j-1}}^{t^j}((P_h^1 - I)u_t)^2\ ds\ \Delta t_F\Big] \\ &\leq \frac{1}{\mu}\sum_{j=1}^{n}\int_{t^{j-1}}^{t^j}\left\|(P_h^1 - I)u_t\right\|^2_{L^2(\Omega)}\ ds, \\ &\leq \frac{C}{\mu}h^4\sum_{j=1}^{n}\int_{t^{j-1}}^{t^j}\|u_t\|^2_{H^2(\Omega)}, \text{ by the definition of,} P_h^1 \\ &\leq \frac{C}{\mu}h^4\int_0^{t^n}\|u_t\|^2_{H^2(\Omega)}\ ds. \qquad \text{(B.4)}\end{aligned}$$

– To estimate the L^2 norm of the w_2, we write

$$w_2^j = \frac{1}{\Delta t_F}(u(t^j) - u(t^{j-1})) - u_t(t^j),$$
$$= -\frac{1}{\Delta t_F}\int_{t^{j-1}}^{t^j}(s - t^{j-1})u_{tt}(s)\ ds,$$

such that we end up with

$$\frac{\Delta t_F}{\mu}\sum_{j=1}^{n}\left\|w_2^j\right\|^2_{L^2(\Omega)} \leq \frac{1}{\mu}\sum_{j=1}^{n}\left\|\int_{t^{j-1}}^{t^j}(s - t^{j-1})u_{tt}(s)\ ds\right\|^2_{L^2(\Omega)} \leq \frac{\Delta t_F^2}{\mu}\int_0^{t^n}\|u_{tt}\|^2_{L^2(\Omega)}\ ds.$$

Combining the estimates on ρ and θ concludes the proof. ∎

Appendix C. Remarks on λ_N and $\varepsilon(N)$

Let us start with the N-behavior of the maximum eigenvalue λ_N. First of all let us remind that, in this paper, we have considered h small enough so that all finite element errors are negligible with respect to the target accuracy that is expected. In this spirit, we consider that the reduced modes, and the eigenvalues all converge to "continuous" entities as the finite element discretization improves ($h \to 0$). This allows to state that, what we named X_h^N in the paper almost coincide with the associated "continuous" entities, i.e. the reduced space X_N (similarly, the discrete eigenvalues λ_i are close the their continuous counterparts).

We present in Table C.1 the values of $\sqrt{\lambda_N}$ (more precisely $\sqrt{\lambda_N^h}$) for $N = 1, \ldots, 10$ in both cases, the heat equation and the Brusselator. Of course, all eigenvalues, in particular λ_N, are larger than the inverse of the squared Poincaré constant since for any $v \in H_0^1(\Omega)$, $\|v\|_{L^2(\Omega)} \leq C\,\|\nabla v\|_{L^2(\Omega)}$. More importantly, the maximum eigenvalue appears in the inverse inequality for functions in X_N, meaning that

$$\forall v \in X_N, \quad \|\nabla v\|_{L^2(\Omega)} \leq \sqrt{\lambda_N}\|v\|_{L^2(\Omega)} \tag{C.1}$$

TABLE C.1. Values of $\sqrt{\lambda_N}$ defined in (3.2) and appearing in the inverse inequality (C.1) (for $N = 1, \ldots, 10, 21, \ldots, 30$)

$N =$	1	2	3	4	5	6	7	8	9	10
Heat equation	4.44	8.89	9.94	13.34	14.16	16.04	21.19	22.48	30.95	58.58
Brusselator	0.04	34.85	87.66	131.76	191.78	197.26	199.04	206.96	232.37	233.83
$N =$	21	22	23	24	25	26	27	28	29	30
Heat equation	389.41	389.96	393.61	394.51	395.47	396.52	397.64	400.90	401.50	402.36
Brusselator	294.04	297.39	314.95	324.08	331.77	336.42	341.12	341.61	342.48	342.93

Naturally, $\sqrt{\lambda_N}$ increases with N, however, for both equations, it looks like from our numerical simulations, that it is saturating around 300 - 400. This is consistent with the intuition that, over the set $\mathcal{S}$ of all solutions to the parameter dependent problem ((2.1) or (5.6)), when the parameter varies in some compact set, the inverse inequality, that we conjecture:

Conjecture. $\forall v \in \mathcal{S}$, $\|\nabla v\|_{L^2(\Omega)} \leq C\|v\|_{L^2(\Omega)}$, *holds for some positive constant* C.

We then proceed with $\varepsilon(N)$, i.e. the proxy of the Kolmogorov N-width, given by the error between the elements in $\mathcal{S}$ and their approximation by the orthogonal projection on X_N. Actually, there

are numerous approaches for handling these approximations, which stem from the definition of the projection operators and the norms in which the approximations are evaluated.

We thus introduce the operators Π_N^0 and Π_N^1 defined as the $L^2(\Omega)$ and $H^1(\Omega)$ projection operators on the space X_N spanned by the RB $\{\Phi_i^h\}_{i,\dots,N}$.

Due to the L^2-normalization of the RB, and (3.2), Π_N^0 and Π_N^1 verify

$$\forall u \in L^2(\Omega), \quad \Pi_N^0 u := \sum^N i = 1 (u, \Phi_i^h)_{L^2(\Omega)} \ \Phi_i^h, \quad \text{and} \quad \forall u \in H^1(\Omega), \quad \Pi_N^1 u := \sum_{i=1}^N (u, \Phi_i^h)_{H^1(\Omega)} \ \frac{\Phi_i^h}{\lambda_i}.$$

The assumption we made on $\mathcal{S}$ is that

$$\varepsilon_N^0 := \text{argmax}_{u \in \mathcal{S}} \left\| u - \Pi_N^0 u \right\|_{L^2(\Omega)} \quad \text{and} \quad \varepsilon_N^1 := \text{argmax}_{u \in \mathcal{S}} \left\| u - \Pi_N^1 u \right\|_{H^1(\Omega)}$$

both decrease rapidly (note that $\varepsilon_N^0 \leq \varepsilon_N^1$).

Of interest may also be to consider the quantities (as in the proof of Theorem 4.5 in the present paper), $\varepsilon_N^{1'} := \text{argmax}_{u \in \mathcal{S}} \left\| u - \Pi_N^1 u \right\|_{L^2(\Omega)}$ and $\varepsilon_N^{0'} := \text{argmax}_{u \in \mathcal{S}} \left\| u - \Pi_N^0 u \right\|_{H^1(\Omega)}$.

First of all, let us remark that $\varepsilon_N^{1'} \leq \varepsilon_N^1$, since the $L^2(\Omega)$-norm is upper bounded by the $H^1(\Omega)$-norm. Then, we split $\left\| u - \Pi_N^0 u \right\|_{H^1(\Omega)}$ into two contributions:

$$\begin{aligned}
\left\| u - \Pi_N^0 u \right\|_{H^1(\Omega)} &= \left\| (I - \Pi_N^1) u + (\Pi_N^1 - \Pi_N^0) u \right\|_{H^1(\Omega)}, \\
&\leq \left\| (I - \Pi_N^1) u \right\|_{H^1(\Omega)} + \left\| (\Pi_N^1 - \Pi_N^0) u \right\|_{H^1(\Omega)}, \\
&\leq \varepsilon_N^1 + \sqrt{\lambda_N} \left\| (\Pi_N^1 - \Pi_N^0) u \right\|_{L^2(\Omega)}, \text{from (C.1)} \\
&\leq \varepsilon_N^1 + \sqrt{\lambda_N} (\varepsilon_N^0 + \varepsilon_N^{1'}).
\end{aligned}$$

which yields

$$T_2 = \left\| u_h^n(\mu) - \sum_{i=1}^N (u_h^n(\mu), \Phi_i^h) \ \Phi_i^h \right\|_{H^1(\Omega)} \leq \varepsilon'(N), \tag{C.2}$$

with $\varepsilon'(N) \leq \varepsilon_N^1 + \sqrt{\lambda_N}(\varepsilon_N^0 + \varepsilon_N^{1'})$. In addition if $\varepsilon_N^0 \simeq \varepsilon_N^{1'}$, we obtain

$$T_2 \leq \varepsilon_N^1 + 2\sqrt{\lambda_N} \varepsilon_N^0.$$

In order to better appreciate the different behaviours of ε_N^0, ε_N^1, $\varepsilon_N^{0'}$ and $\varepsilon_N^{1'}$ we have performed some numerical experiments on these quantities, both for the heat equation and the Brusselator. We report in Figures C.1 and C.3, the N-convergence concerning ε_N^0 and $\varepsilon_N^{1'}$ for both cases. We can see that both quantities are rapidly decreasing, at about the same rate. Similarly, we report in Figures C.2 and C.4, the N-convergence for $\varepsilon_N^{0'}$ and ε_N^1 in both cases. We can see that these quantities are rapidly decreasing, at about the same rates for ε_N^0 and $\varepsilon_N^{1'}$ on the one hand and ε_N^1 and $\varepsilon_N^{0'}$ on the other hand. Second, we observe that the ratio between these quantities scale as one might expect, i.e. $\sqrt{\lambda_N}\varepsilon_N^0 \simeq \varepsilon_N^1$ (but this is just a conjecture, not so important in the frame of this paper).

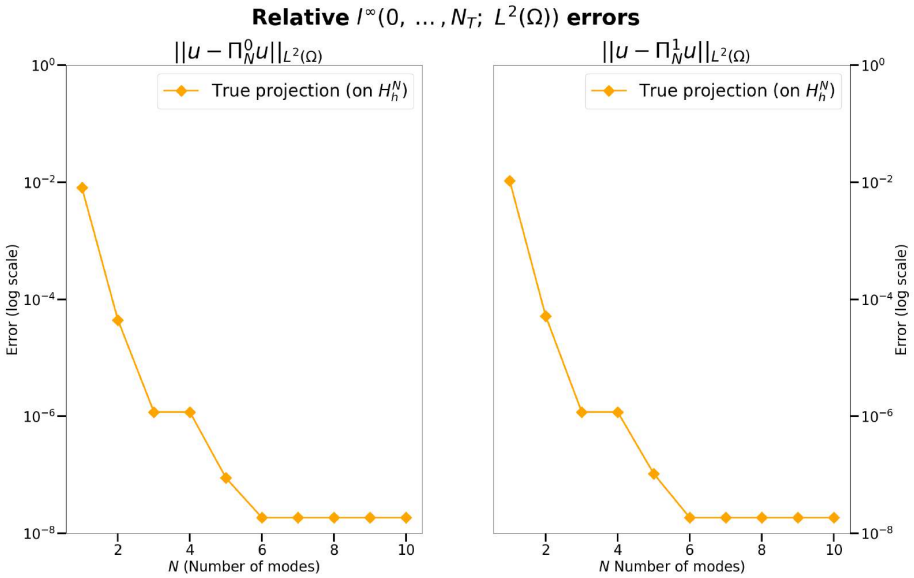

FIGURE C.1. Heat equation: relative error for ε_N^0 (left) and $\varepsilon_N^{1'}$ (right) as a function of $N = 1, \ldots, 30$ with $h = 0.01$

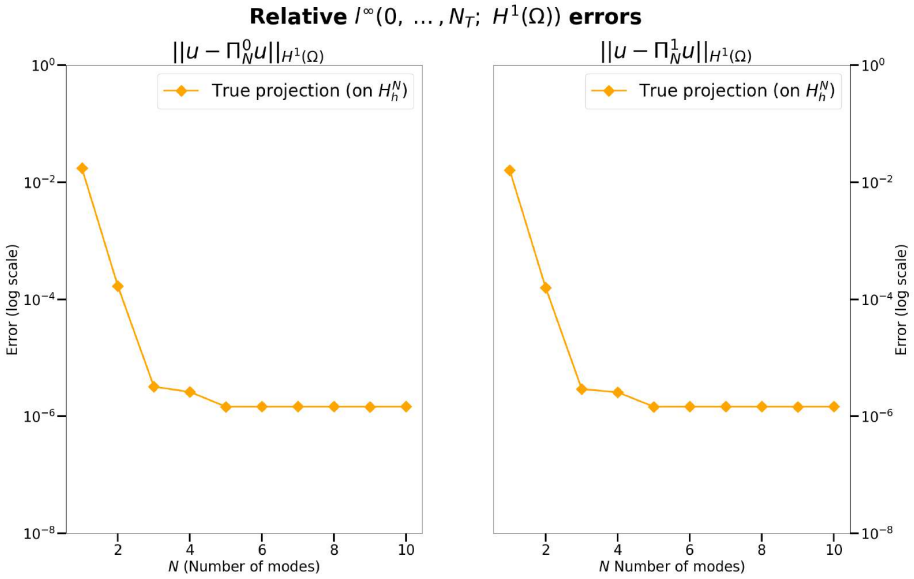

FIGURE C.2. Heat equation: relative error for $\varepsilon_N^{0'}$ (left) and ε_N^1 (right) as a function of $N = 1, \ldots, 30$ with $h = 0.01$

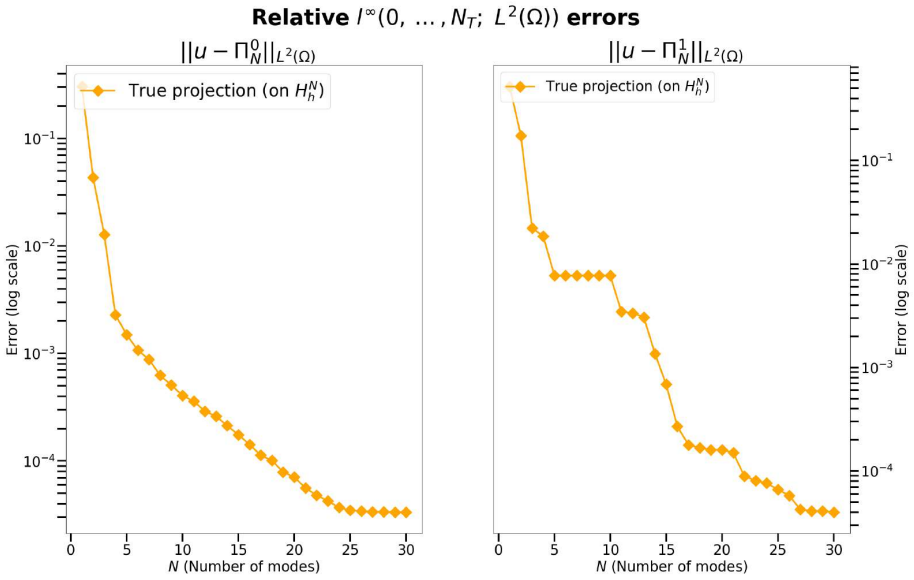

FIGURE C.3. Brusselator: relative error for ε_N^0 (left) and $\varepsilon_N^{1'}$ (right) as a function of $N = 1, \ldots, 30$ with $h = 0.02$

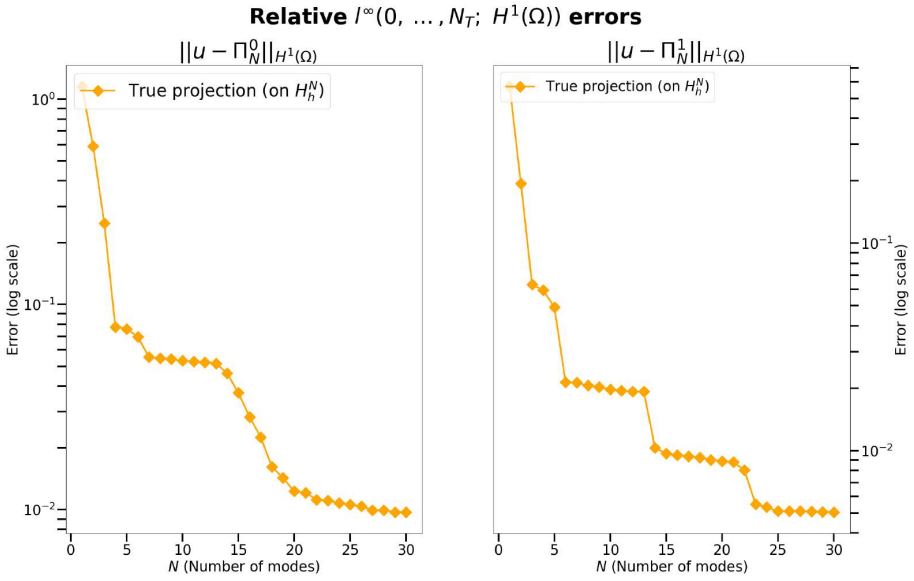

FIGURE C.4. Brusselator: relative error for $\varepsilon_N^{0'}$ (left) and ε_N^1 (right) as a function of $N = 1, \ldots, 30$ with $h = 0.02$

References

[1] M. Barrault, C. Nguyen, A. T. Patera, and Y. Maday. An 'empirical interpolation' method: application to efficient reduced-basis discretization of partial differential equations. *C. R. Math. Acad. Sci. Paris*, 339-9:667–672, 2004.

[2] G. Berkooz, P. Holmes, and J. L. Lumley. The proper orthogonal decomposition in the analysis of turbulent flows. *Annu. Rev. Fluid Mech.*, 25(1):539–575, 1993.

[3] S. Brenner and R. Scott. *The mathematical theory of finite element methods*, volume 15. Springer, 2007.

[4] A. Buffa, Y. Maday, A. T. Patera, C. Prud'Homme, and G. Turinici. A priori convergence of the Greedy algorithm for the parametrized reduced basis method. *ESAIM, Math. Model. Numer. Anal.*, 46(3):595 – 603, 2012.

[5] N. Cagniart, Y. Maday, and B. Stamm. Model order reduction for problems with large convection effects. In *Contributions to partial differential equations and applications*, volume 47 of *Computational Methods in Applied Sciences*, pages 131–150. Springer, 2019.

[6] F. Casenave, A. Ern, and T. Lelièvre. A nonintrusive reduced basis method applied to aeroacoustic simulations. *Adv. Comput. Math.*, 41(5):961–986, 2014.

[7] R. Chakir. *Contribution à l'analyse numérique de quelques problèmes en chimie quantique et mécanique.* PhD thesis, Université Pierre et Marie Curie-Paris VI, 2009.

[8] R. Chakir and Y. Maday. A two-grid finite-element/reduced basis scheme for the approximation of the solution of parametric dependent P.D.E. In *Actes du 9e Colloque national en calcul des structures, Giens*, 2009.

[9] R. Chakir, Y. Maday, and P. Parnaudeau. A non-intrusive reduced basis approach for parametrized heat transfer problems. *J. Comput. Phys.*, 376:pp.617–633, 2019.

[10] R. Chakir, B. Streichenberger, and P. Chatellier. A Non-Intrusive Reduced Basis Method for Urban Flows Simulation. In *WCCM-ECCOMAS'20, 14th World Congress of Computational Mechanics and 8th European Congress on Computational Methods in Applied Sciences and Engineering*, page 12p, 2021.

[11] W. Chen, J. S. Hesthaven, B. Junqiang, Y. Qiu, Z. Yang, and Y. Tihao. Greedy nonintrusive reduced order model for fluid dynamics. *AIAA J.*, 56(12):4927–4943, 2018.

[12] J. Duan and J. S. Hesthaven. Non-intrusive data-driven reduced-order modeling for time-dependent parametrized problems. `https://arxiv.org/abs/2303.02986`, 2023.

[13] L. C. Evans. *Partial differential equations.* American Mathematical Society, 2010.

[14] S. Fresca and A. Manzoni. Pod-DL-ROM: enhancing deep learning-based reduced order models for nonlinear parametrized PDEs by proper orthogonal decomposition. *Comput. Methods Appl. Mech. Eng.*, 388: article no. 114181 (27 pages), 2022.

[15] R. Geelen, S. Wright, and K. Willcox. Operator inference for non-intrusive model reduction with nonlinear manifolds. `https://arxiv.org/abs/2205.02304`, 2022.

[16] E. Grosjean. *Variations and further developments on the Non-Intrusive Reduced Basis two-grid method.* PhD thesis, Mathématiques Appliquées Sorbonne Université, 2022.

[17] E. Grosjean and Y. Maday. Error estimate of the non-intrusive reduced basis method with finite volume schemes. *ESAIM, Math. Model. Numer. Anal.*, 55(5):1941–1961, 2021.

[18] E. Grosjean and B. Simeon. The non-intrusive reduced basis two-grid method applied to sensitivity analysis. `https://arxiv.org/abs/2301.00761`, 2023.

[19] M. Guo and J. S. Hesthaven. Data-driven reduced order modeling for time-dependent problems. *Comput. Methods Appl. Mech. Eng.*, 345:75–99, 2019.

[20] B. Haasdonk. Convergence rates of the pod–greedy method. *ESAIM, Math. Model. Numer. Anal.*, 47(3):859–873, 2013.

[21] B. Haasdonk and M. Ohlberger. Reduced basis method for finite volume approximations of parametrized linear evolution equations. *ESAIM, Math. Model. Numer. Anal.*, 42(2):277–302, 2008.

[22] W. Haik, Y. Maday, and L. Chamoin. A real-time variational data assimilation method with data-driven model enrichment for time-dependent problems. *Comput. Methods Appl. Mech. Eng.*, 405: article no. 115868 (37 pages), 2023.

[23] F. Hecht. New development in FreeFem++. *J. Numer. Math.*, 20(3-4):251–266, 2012.

[24] J. S. Hesthaven, C. Pagliantini, and G. Rozza. Reduced basis methods for time-dependent problems. *Acta Numer.*, 31:265–345, 2022.

[25] J. S. Hesthaven, G. Rozza, and B. Stamm. *Certified reduced basis methods for parametrized partial differential equations*. Springer, 2016.

[26] D. J. Knezevic and A. T. Patera. A certified reduced basis method for the Fokker–Planck equation of dilute polymeric fluids: FENE dumbbells in extensional flow. *SIAM J. Sci. Comput.*, 32(2):793–817, 2010.

[27] A. Kolmogoroff. Über die beste Annaherung von Funktionen einer gegebenen Funktionenklasse. *Ann. Math.*, pages 107–110, 1936.

[28] J.-L. Lions and E. Magenes. Problemes aux limites non homogenes. II. *Ann. Inst. Fourier*, 11:137–178, 1961.

[29] Y. Maday and B. Stamm. Locally adaptive greedy approximations for anisotropic parameter reduced basis spaces. *SIAM J. Sci. Comput.*, 35(6):A2417–A2441, 2013.

[30] R. C. Mittal and R. Jiwari. Numerical solution of two-dimensional reaction–diffusion Brusselator system. *Appl. Math. Comput.*, 217(12):5404–5415, 2011.

[31] C. Prud'Homme, V. Chabannes, V. Doyeux, M. Ismail, A. Samake, and G. Pena. Feel++: A computational framework for galerkin methods and advanced numerical methods. In *ESAIM: Proceedings*, volume 38, pages 429–455. EDP Sciences, 2012.

[32] A. Quarteroni, A. Manzoni, and F. Negri. *Reduced Basis Methods for Partial Differential Equations: an introduction*, volume 92. Springer, 2015.

[33] B. Streichenberger. *Approches multi-fidélités pour la simulation rapide d'écoulements d'air en milieu urbain.* PhD thesis, Université Gustave Eiffel, 2021.

[34] V. Thomée. *Galerkin finite element methods for parabolic problems*, volume 25. Springer, 2007.

[35] D. Xiao, F. Fang, C. Pain, and G. Hu. Non-intrusive reduced-order modelling of the Navier–Stokes equations based on RBF interpolation. *Int. J. Numer. Methods Fluids*, 79(11):580–595, 2015.